

Assessing salt precipitation and weak acid interaction in subsurface CO₂ injection: Potential 50% strength decline in near-wellbore reservoir sandstones

Mohammad Nooraiepour¹, Krzysztof Polański², Mohammad Masoudi¹, Szymon Kuczyński², Hannelore Derluyn³, Liebert Parreiras Nogueira⁴, Bahman Bohloli⁵, Stanislaw Nagy² and Helge Hellevang¹

¹ Department of Geosciences, University of Oslo, P.O. Box 1047 Blindern, 0316 Oslo, Norway

² AGH University of Kraków, Mickiewicza 30 Av, 30-059 Kraków, Poland

³ Universite de Pau et des Pays de l'Adour, E2S UPPA, CNRS, LFCR, Pau, France

⁴ Oral Research Laboratory, Institute of Clinical Dentistry, University of Oslo, Oslo 0317, Norway

⁵ Norwegian Geotechnical Institute (NGI), Sognsveien 72, Oslo, 0855, Norway

* Corresponding author: mohammad.nooraiepour@geo.uio.no

Abstract

Predictive modeling of CO₂ storage sites requires a detailed understanding of physico-chemical processes and potential challenges for scale-up. Dramatic injectivity decline may occur due to salt precipitation pore clogging in high-salinity reservoirs, even over a short time frame. This study aims to elucidate the adverse impact of CO₂-induced salt crystallization in porous media on the geomechanical properties of near-wellbore reservoir sandstones. As the impact of salt precipitation cannot be isolated from the precursor effects of interaction with CO₂ and carbonic acid, we initiated our study by comprehensive review of CO₂ chemo-mechanical interactions with sandstones. We conducted laboratory geochemical CO₂-brine-rock interactions at elevated pressures and temperatures on two sets of porous sandstone with contrasting petrophysical qualities. Two paths were followed: treatment with (a) CO₂-acidified brine at 10 MPa fluid pressure and 60 °C for 7 days, and a second subset continuation with (b) supercritical injection until complete dry-out and salt precipitation. Afterward, the core samples were tested in a triaxial apparatus at varying stresses and temperatures. The elastic moduli of intact, CO₂-reacted, and salt-damaged sandstones were juxtaposed to elucidate the extent of crystallization damages. The salt-affected specimens showed a maximum of 50% reduction in Young's and shear moduli and twice an increase in Poisson's ratio compared to intact condition. The deterioration was notably higher for the tighter rocks with higher initial stiffness.

Keywords: Review; Salt precipitation; Geochemical reaction; Fluid-Rock interaction; Geomechanical properties; Geological carbon storage

1. Introduction

Achieving a significant and timely reduction in global greenhouse gas emissions is a major challenge for modern human civilization. There is growing consensus that an essential part of the solution to mitigate climate change is the deployment of long-term subsurface storage of carbon dioxide (CO₂) in geological formations (IPCC, 2023), a technological chain of processes referred to as Carbon Capture and Storage (CCS), Geological CO₂ Storage (GCS), or CO₂ sequestration. Among the various opportunities for atmospheric CO₂ emission reductions, such as a blend of more renewable energy, improved energy efficiency, CCS contribution is anticipated to be around 10-15% of total cumulative emissions reductions through 2050, which is approximately 120 Gigatons (Gt) (IEA, 2016; Ringrose et al., 2021). The IPCC AR6 Synthesis Report refers to CCS technology as a critical CO₂ mitigation

option. In 1.5°C Special Report, three of the four pathways involve significant use of CCS (350 to 1200 gigatons stored by 2100), mandating radical changes in human behavior in the last pathway without CCS deployment. The required subsurface storage rate need to be 6–7,000 million tons annually in 2050 (IEA, 2015; Ringrose and Meckel, 2019). It has been argued that GCS in saline aquifers enables delivering the long-term expectations for CCS and realizing the 2-degree scenario (2DS) goals (Ringrose and Meckel, 2019), while GCS in petroleum reservoirs and mafic/ultramafic rocks (e.g., basalt) will play an important role in some geographic locations.

Given the expected enormous annual injection of CO₂ in saline aquifers with varying salinity and petrophysical properties, it is critical to delineate dominant physicochemical processes that occur during saline aquifer storage. Injected CO₂ in geological formations disturbs the existing equilibrium between formation brine and rock-forming minerals, acidifies the resident brine, triggers (geo)chemical reactions, and accelerates fluid-rock interactions in porous media, which may alter the mechanical and hydraulic properties of the reservoir and caprock layers (Liu et al., 2012; Masoudi et al., 2024; Nooraiepour et al., 2022; Pham et al., 2011; Rohmer et al., 2016; Vafaie et al., 2023). Out of potential thermo-hydro-mechanical-chemical (THMC) coupling during GCS, we focus on chemically-induced alterations of rocks. In particular, changes in geomechanical properties of reservoir rocks in hypersaline aquifers in the regions near injection wells. The distinction between the consequences of CO₂-induced salt precipitation in porous media that comes into effect after collective impacts of interactions with pure CO₂ and CO₂-acidified brine is challenging to establish reliably. Our introduction thus initiates with a comprehensive literature review, followed by a parallel exploration in our experiments.

Table 1 (Refer to Appendix) presents an overview of research on chemo-mechanical interactions of CO₂ (dry, wet, and water/brine-acidified) only with sandstone rock type. The literature indicates that the geomechanical properties of CO₂-reacted sandstones experience deterioration. This includes elastic parameters (Young's modulus, bulk modulus, shear modulus, and Poisson's ratio), strength, failure and deformation responses, creep properties, stress-strain behavior, and rock physics properties. This degradation is particularly noticeable when geochemical reactions (involving fluid-rock interactions) occur under elevated temperature-pressure conditions, such as those found at reservoir conditions, and extend over prolonged experimental periods. However, the above-mentioned consequences and their severity are not unanimous, particularly when carbonate-lean sandstones (as clastic grains or intergranular cement) are evaluated (refer to Table 1). The decline in mechanical strength, often rooted in the debilitation of grain bonding, results in the geomechanical weakening of reservoir rocks. The presence of impurities such as SO_x, NO_x, in addition to supercritical CO₂ (ScCO₂) has been shown to result in enhanced weakening in rock mechanical properties (Erickson et al., 2015). Subsurface CO₂ injection also changes the stress regime in the storage reservoirs and overlying caprocks, particularly in the near-wellbore regions (Rahman et al., 2022; Rutqvist et al., 2008; Vilarrasa et al., 2014). Deteriorated strength and stiffness parameters (physical and mechanical properties) come into play when evaluating safe and secure GCS (Nooraiepour et al., 2017; Song and Zhang, 2013; Watts, 1987).

Type, extent, and kinetics of chemical reactions (or fluid-rock interactions) may vary across zones with different distances from the wellbores as a function of the volumetric fraction of aqueous phases (brine) and CO₂ in porous media, and the mutual concentration of dissolved water and CO₂ in each other (Rohmer et al., 2016; Vafaie et al., 2023). In other words, fluid phase saturation in pore structures controls interactions (Kampman et al., 2014; Miri and Hellevang, 2016; Nooraiepour, 2018). In the

nearest region to the wellbore, dry ScCO₂ occupies most of the reservoir pore volume. The low chemical reactivity of ScCO₂ during continuous injection may sweep out the brine pore fluid, dry out the region, and cause precipitation and growth of salt crystals (Masoudi et al., 2021; Miri and Hellevang, 2016; M Nooraiepour et al., 2019). The next region around the injection well represents a zone of water-bearing ScCO₂ or saturated/wet ScCO₂. In contrast to dry ScCO₂, it shows a reactive nature enhancing surface/interface (geo)chemical processes on rock-forming minerals (Lin et al., 2008; Loring et al., 2011; Pearce et al., 2016). This zone is followed by an extended region where two fluids (brine and ScCO₂) coexist at varying proportions. In all these three regions, CO₂ dissolution in brine leads to carbonic acid generation (H₂CO₃), which dissociates into aqueous protons (H⁺), leading to a pH drop to an acidic range of 3.5–5.0 (Gaus, 2010). It, in turn, induces subsequent surface/interface-coupled mineral dissolution and precipitation (An et al., 2021; Chen et al., 2014; Deng et al., 2022; Fazeli et al., 2019b, 2019a; Guren et al., 2020; Prasianakis et al., 2017).

Acidified pore water can cause changes in the pore geometry of reservoir rocks and bring about mineral dissolution and precipitation. The resulting pore morphology alteration affects the rock porosity and permeability (i.e., porous media hydrodynamics) and, eventually, the mechanical properties and strength of the targeted storage sites (Kim and Santamarina, 2014; Nooraiepour, 2018; Vafaie et al., 2023; Zhang et al., 2016). The volumetric content and spatial distribution of reactive minerals, in addition to the porous structure and fluid flow condition, will determine which rock properties may change. CO₂-fluid-rock interactions have been thoroughly studied in the past two decades. For instance, refer to the reviews conducted by Czernichowski-Lauriol et al. (1996), Gaus (2010), Zhang and Bachu (2011), Song and Zhang (2013), Rohmer et al. (2016), and Vafaie et al. (2023). Interaction with CO₂-acidified water leads to enhanced chemical reactions in carbonates, whereas the acidity of the injected fluid is expected to have a less adverse impact on anhydrites, clay-rich caprocks, and sandstones.

The composition of intergranular cement in sandstones can play a remarkable role in the rock properties evolution, i.e., silicate or calcite cementation. Carbonate-cemented reservoir sandstones are susceptible to enhancements in dissolution-induced porosity (and permeability) (Espinoza et al., 2018; Fazeli et al., 2019a; Rathnaweera et al., 2017; Wu et al., 2018). In particular, under advective (open flow) conditions hindering buffering effects (Fazeli et al., 2019a, 2019b). Additionally, studying outcrops and natural-analog specimens exposed to CO₂ migration over geological time documented a porosity increase due to the dissolution of grain-coating hematite and calcite cement. The dissolution rate of sandstone grains, which often constitute quartz, feldspar, and clay grains are markedly slower than carbonates, particularly calcite (Brantley et al., 2008; Palandri and Kharaka, 2004). Nevertheless, as documented in several laboratory and numerical experiments, low-carbonate sandstones containing clays and feldspars are more reactive with dissolved CO₂ over longer times than quartz grains (Hangx and Spiers, 2009; Pham et al., 2011; Tutolo et al., 2015; Zhu et al., 2019).

A CO₂-brine-rock interaction that is rapid and relevant for injection-timescales, is the CO₂-induced salt precipitation, which is geochemical reaction with potentially significant consequences in the near-wellbore regions is CO₂-induced salt precipitation. Injection of large volumes of undersaturated ScCO₂ leads to the evaporation of the formation water and an increase in the concentration of the dissolved salts in brine pore fluid. Under the thermodynamic conditions of a given storage reservoir, solute concentration will eventually reach the solubility limit and precipitate out of the aqueous phase, leading

to salt precipitation inside the porous reservoir rocks (Falcon-Suarez et al., 2020; Miri and Hellevang, 2016; Mohammad Nooraiepour et al., 2018; Norouzi et al., 2022; Ott et al., 2021; Parvin et al., 2020). This study primarily investigates subflorescence (salt crystallization inside the material), contrasting efflorescence (surface growth).

In construction, rock slope stability, and cultural heritage preservation, salt crystallization in porous materials, often called salt weathering, is considered one of the significant causes of rock decay in nature and man-made materials (Desarnaud et al., 2013; Flatt et al., 2017; Lubelli et al., 2023). It has been shown that salt precipitation in porous media and microcavities (representing confined spaces) has the potential to exert sufficient stress to overcome the tensile strength of most rocks, alter their pore space, induce microcracks, and change mechanical properties (Derluyn et al., 2014; Desarnaud et al., 2016; Shahidzadeh-Bonn et al., 2010). During surface salt weathering, repeated dissolution-recrystallization of salt in rock pore volumes is the root cause of rock damage, fragmentation and disintegration (Derluyn et al., 2019; Godts et al., 2021). However, not much research has been published on the potential adverse impact of CO₂-induced salt precipitation on the geomechanical properties of reservoir rocks in the near-wellbore vicinity. There is also literature speculating that mineral precipitation in porous media during GCS operation may instead increase strength (Rosenbauer et al., 2005).

In high-salinity GCS reservoirs (i.e., hypersaline aquifers), dramatic injectivity decline might be expected due to salt precipitation and continued growth resulting in pore clogging, even in the short-term. Therefore, this study aims to address this knowledge need and elucidate the discrepancy in the positive/negative impact of mineral precipitation (particularly salt subflorescence) in porous media on the geomechanical properties of storage reservoirs. We conducted batch-type interaction of sandstone samples with ScCO₂-acidified high salinity sodium chloride brine, and then flow-through ScCO₂ injection until salt crystallization and dry-out of porous rocks both at elevated temperatures. Mechanical behavior and elastic moduli of unreacted (intact) and two sets of reacted (i. with ScCO₂-acidified brine, and ii. those followed until salt precipitation) sandstone cores were then compared using high-pressure high-temperature (HPHT) triaxial geomechanical experiments. Additionally, two sets of distinct petrophysical quality representing diverse pore structures were studied to provide insight into the range of impacts of in-pore salt crystallization and growth.

2. Materials and Methods

2.1. Sample preparation

Two Berea-class sandstone core samples with distinct petrophysical quality were selected. The porosity (φ) and permeability (k) for the Boise Buff (BB) sandstones are 25-28% and 1000 mD (σ = 700-3000 mD), representing excellent reservoir quality index (RQI). The respective petrophysical properties for the Torrey Red (TR) core samples with low to medium RQI are φ = 13-16% and 1 mD (σ = 0.2-2 mD). For each reservoir rock type, we acquired ten cylindrical core plugs perpendicular to the bedding with dimensions of approximately 38.1 mm (1 1/2") in diameter and approximately 76.2 mm (3") in height.

2.2. Sample characterization

The whole-rock (bulk) mineralogical composition was identified and quantified using X-ray diffraction (XRD) technique. The composition was verified using an in-house automated mineralogy and petrography mapping module under energy-dispersive x-ray spectroscopy (EDS) integrated into scanning electron microscopy (SEM). The EDS analysis was used for the identification of chemical elements and surface composition mapping. High-resolution SEM imaging via backscattered (BSE) and secondary electrons (SE) was carried out to study grain-pore distribution, surface geometries in addition to salt growth. The detailed XRD and SEM-EDS procedures have been given in Nooraiepour et al. (2017a,b) and Nooraiepour et al. (2021a,b), respectively.

Three-dimensional (3D) tomograms were recorded for intact, CO₂-reacted, and salt-damaged sandstones. The x-ray computed tomography (micro-CT) was performed using a Bruker Multiscale SkyScan 2211 at 110 kV, 65 μ A, and an exposure time of 400 ms, averaging 5 frames per projection. The entire set of tomograms was taken over a 360° rotation with a rotation step of 0.29° (1242 projections). These settings resulted in a final voxel size of 12 μ m. Micro-CT projections were reconstructed using the proprietary NRecon hierarchical 3D reconstruction software, including ring artifact and beam hardening correction. The resulting reconstructions were then visualized and analyzed using the Dragonfly software (v. 2022.2, Comet Technologies Canada Inc.). The virtual slices were pre-processed to remove distorted outer regions and filtered with artifact attenuation (gradient domain fusion), and non-local means denoising filters. The slices were then segmented into distinct phases with visual thresholds (Otsu algorithm) to define seeds for the watershed algorithm based on the grey-scale gradient and grey-scale intensity of each voxel. The outcome was then used for quantifying each phase's spatial distribution and volumes.

2.3. Geochemical fluid-rock interaction

In addition to performing geomechanical experiments on intact (unreacted) BB and TR sandstones, the effects of potential geochemical reactions with CO₂-acidified brine on the mechanical properties of CO₂ storage reservoir rocks were studied. A total of 10 natural core samples were tested from BB and TR reservoir units. Following the testing of 3/4 intact samples, we selected independent BB and TR sets, each comprising 3 core samples, to explore processes that may take place during CO₂ sequestration in high-salinity aquifers:

- I. Geochemical reaction with CO₂-acidified brine (pressurized supercritical CO₂ dissolved in high-salinity brine) over time at high-pressure high-temperature (HPHT) condition
- II. Continuation of path I with the injection of supercritical CO₂ until evaporation of brine saturation, salt crystal precipitation and growth, and eventually dry out of core sample

Reaction path I simulates generic conditions in hypersaline aquifers, whereas path II focuses on probable scenarios near the CO₂ injection well. Four of the ten core samples prepared from BB and TR sandstones were tested at intact (unreacted) condition and six were tested after geochemical reactions (three samples per reaction path).

We used an HPHT core flooding system (AFS 200, Core Laboratories) to carry out brine-rock chemical interactions with pressurized CO₂ under reservoir conditions. The fluid flow apparatus is equipped with a forced convection benchtop oven (Despatch LBB series), which combines horizontal and vertical airflow and provides temperature uniformity within the air bath. The fluid injection system comprises multiple syringe pumps (Teledyne Isco) supplemented with a backpressure regulator and overburden pressure pump. Two stainless steel fluid accumulators (transfer vessel) and a Hassler-type

core holder within the oven enabled us to equilibrate and inject brine and ScCO₂ phases during paths I and II geochemical interactions. For further details of the experimental setup, refer to Moghadam et al. (2019) and Nooraiepour et al. (2018).

An aqueous solution of 3.4 M (200 g/L) sodium chloride was prepared by adding NaCl (ACS reagent grade, EMSURE) to deionized water (Milli-Q water). A bottle provided grade 5.2 scientific carbon dioxide for preparing CO₂-charged brine and injecting supercritical CO₂ (ScCO₂) into the porous sandstone samples. In path I, the core samples were kept at 10 MPa fluid pressure and 60 °C for 7 days. Path II continued by injecting dry ScCO₂ at 10 MPa injection pressure (constant flow regime, 20 ml/min) into the core sample until brine dry out.

2.4. Geomechanical triaxial compression

The intact and reacted BB and TR sandstones were tested in a servo-hydraulic operated system for triaxial rock mechanical measurements (AutoLab 2000 at AGH University Laboratory). The triaxial apparatus allows controlling pore pressure, confining pressure, and deviatoric stress on cylindrical samples independently with operational limits of 140, 140, and 200 MPa, respectively. In the triaxial apparatus, the maximum limit for axial loading is 1890 kN. The specimen is mounted in a sealed flexible membrane, preventing contact between the confining fluid and the specimen (here, oil was used). Two linearly variable displacement transducers (LVDTs) measured the sample deformation in the axial direction. Another LVDT sensor measured the radial deformation of the specimen. At each stress level, the vertical (or axial) strain was calculated by dividing the measured axial displacement over the initial height of the specimen. The horizontal (or radial) strain was computed by dividing the changes in the specimen's diameter over the specimen's initial diameter. For further details refer to Sharifi et al. (2021, 2023).

To maintain uniform saturation conditions, wherein complete dry-out and salt precipitation necessitate desiccation of the pore fluid, all three scenarios (intact, CO₂-acidified brine treated, and salt crystallization-affected) were examined under dry pore space conditions. Two sets of short-term loading cycles were carried out using the following test protocols:

- A. non-destructive testing to determine Young's modulus and Poisson's ratio during the sample loading was repeated several times at three different temperatures 40, 60, and 80 °C for a given value of confining pressure (5, 10 and 15 MPa). Young's Modulus was determined as tangent modulus where the point of tangency falls within the linear range of the stress-strain curve, approximating inclination of linear elastic deformation. First, the confining pressure was set to a predefined value. The axial load was then controlled by changing the pressure exerted by the piston loading the sample. The amplitude of this load was 2 MPa. After reaching 2 MPa, the load was removed. A 0.1 MPa/s loading rate was adopted for the tests.
- B. destructive tests where the confining pressure applied to the sample was set at 15 MPa. Then, the sample was loaded with the vertical stress exerted by the piston until the sample strength limit was reached. The test continued until the stress was 100% higher than the sample failure stress, and the load was then reduced. The axial displacement rate was 0.01 mm/s.

3. Results and Discussion

3.1. Sample characterization

Figure 1 presents optical images, x-ray micro-computed tomography, scanning electron microscopy, x-ray diffraction patterns of Boise Buff (BB) and Torrey Red (TR) sandstones' pore and matrix structures. It visualizes how different these two reservoir representative core samples are manifested in their respective sedimentary facies' classifications and reservoir quality.

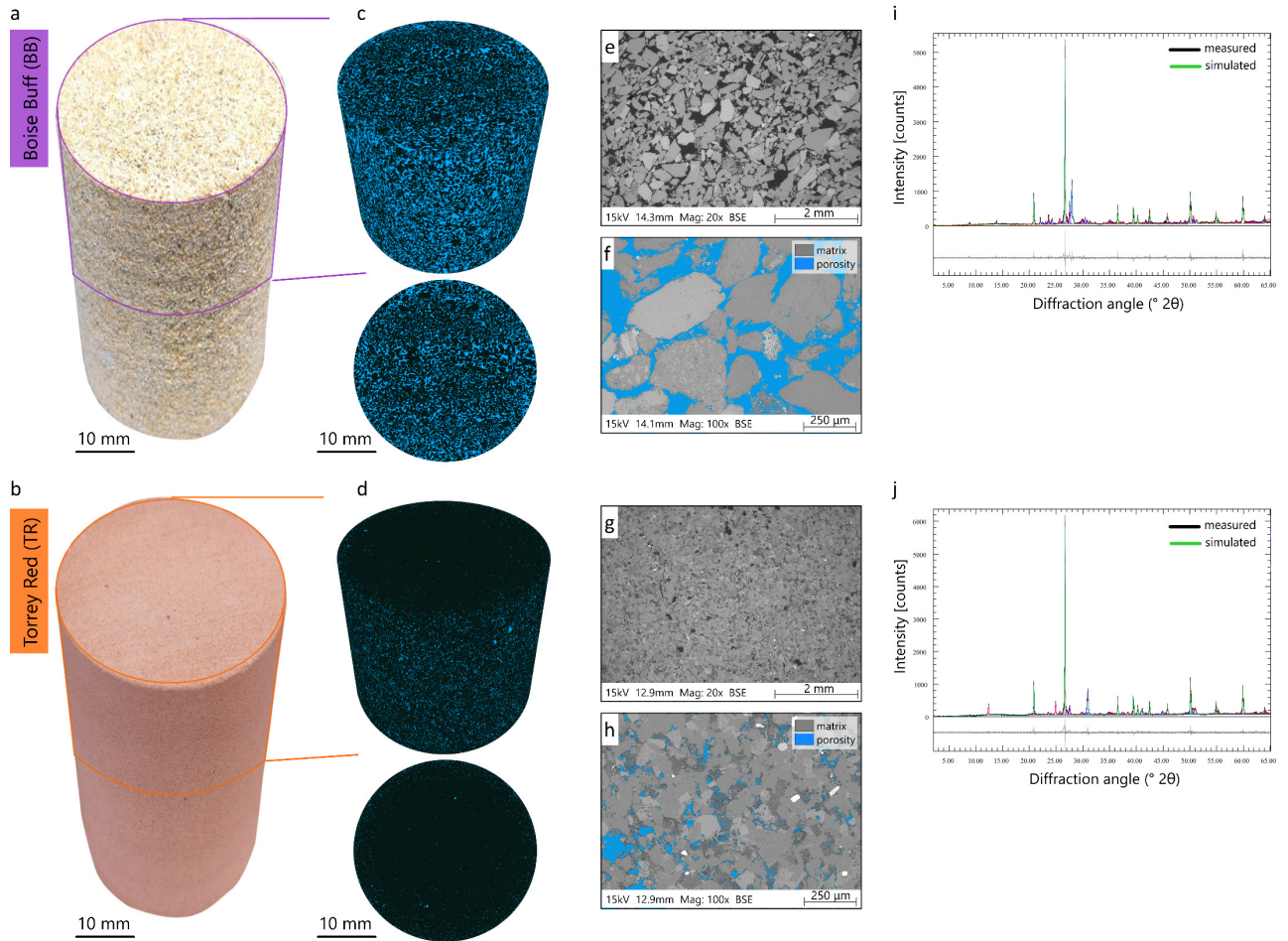


Figure 1. Sample characterization of tested (top) Boise Buff (BB) and (bottom) Torrey Red (TR) reservoir sandstones. (a-b) optical image, (c-d) segmented x-ray micro-computed tomography, (e-h) scanning electron microscopy, (i-j) x-ray diffraction pattern. The subplots visually convey the distinct properties of these two reservoir representative core samples, reflecting their sedimentary facies and petrophysical properties. The interpreted XRD patterns are given in Table 2.

There is a distinct difference between the pore and grain characteristics of the BB and TR sandstones. The BB sandstone shows coarser matrix grains, better sorting, less cementation, bigger intergranular porosity, and better pore connectivity than TR (Fig. 1). The amount of pore-filling material resulting in deteriorated percolating flow pathways is notably higher in TR sandstones. The smaller grain size of TRs results in smaller throat sizes, contributing to lower fluid permeability. The higher compaction level (combination of mechanical and chemical) suggests that TR sandstones are mechanically more competent than BBs.

The whole-rock (bulk) mineralogical composition of reservoir sandstones is presented in Table 2, showing that the BB and TR core samples consist mainly of quartz, feldspar (plagioclase and microcline) with minor amounts of clay, carbonate, and mica (muscovite). The major difference

between the BBs and TRs is notably higher plagioclase (27%) with minor kaolinite clay content (2 %) in BBs. The TRs on the other hand contrasts with 12% kaolinite and approximately 8% dolomite content.

Table 2. Averaged mineralogical composition of Boise Buff (BB) and Torrey Red (TR) sandstones, based on XRD quantitative mineral analysis.

	Quartz	Plagioclase	Microcline	Muscovite	Kaolinite	Dolomite	minor others
Boise Buff (BB)	51	27	17	2	2	0	< 1
Torrey Red (TR)	50	6	22	1	12	8	< 1

3.2. Stress-strain relationship

Figure 2 presents the relationship between stress [MPa] and strain [milistrain] during triaxial compression experiments, in which the applied stress was gradually increased to measure the BBs and TRs deformation. Axial, radial, and volumetric strains are shown in the triaxial setting. The presented test results correspond to the continuous increase in applied stress until failure (fracture development). This provides the peak strength of the studied porous rocks. The stress-strain curves also determine the tentative elastic domain range and yield strength for the tested specimens.

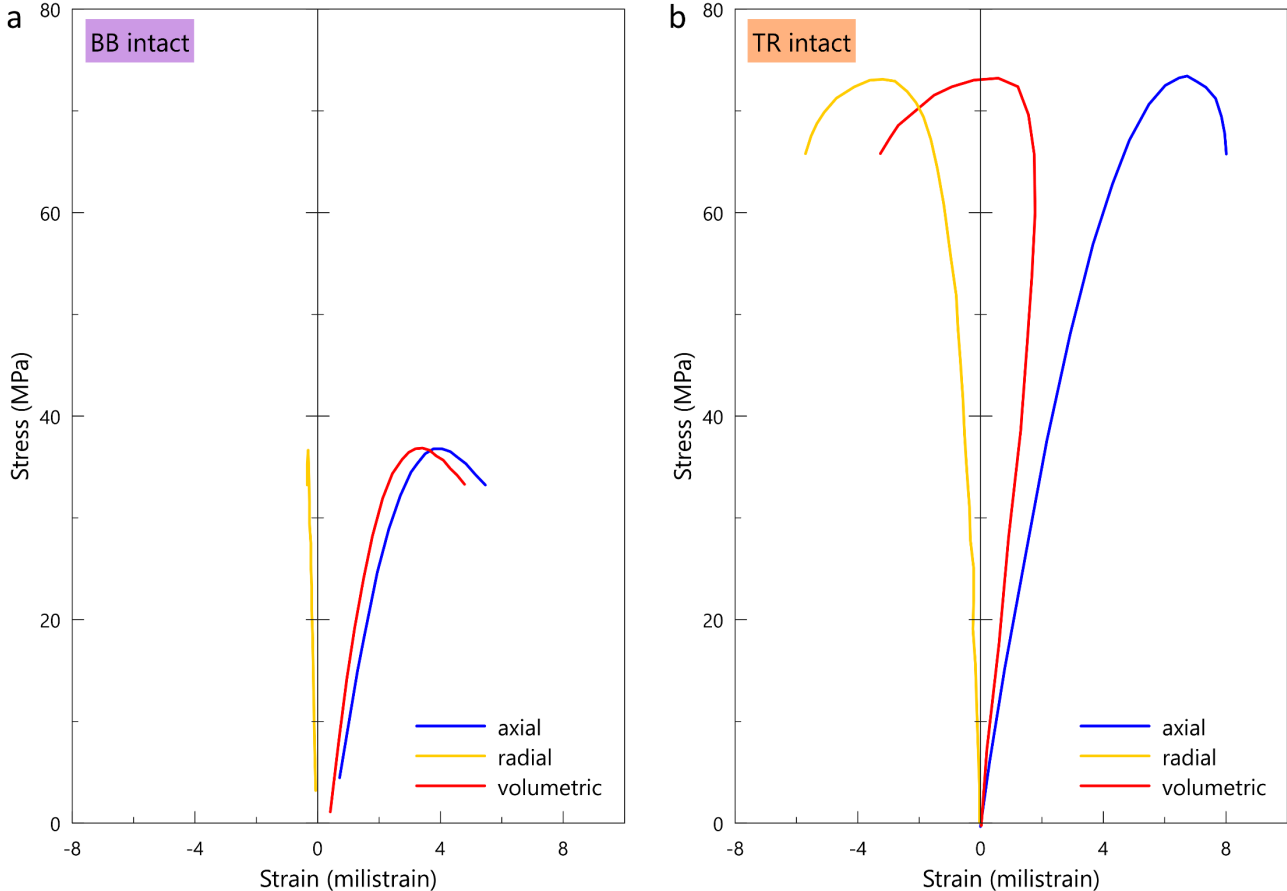


Figure 2. Stress [MPa] versus strain [milistrain] relationship during triaxial compression experiments on intact (a) Boise Buff (BB) and (b) Torrey Red (TR) sandstones. The subplots depict the development of axial, radial, and volumetric strains in the triaxial setting.

As subplots of Figure 2 demonstrate, the peak strength of the intact TR sandstones is approximately twice that of intact BB core samples. The measured average compressive strength of BB and TR reservoir sandstones are approximately 31 and 77 MPa, respectively at 15 MPa confining pressure and 50°C. The less compacted (less cemented) BB reservoir rocks deform relatively faster, reach the yield strength at lower strain levels, and span a more constrained plastic domain before failure (rupture). They also show a very limited radial strain, as depicted in Figure 2a.

The cemented TR sandstones are characterized by notably high mechanical strength in the unreacted condition. The stress-strain curve in the elastic domain develops gently within the elastic deformation domain. The plastic domain is more extended compared to BBs, with a distinction in the plastic deformation signature (Fig. 2b).

3.3. Deformation behavior

3.3.1. Deformation of intact sandstones

Figure 3 presents crossplots of Young's modulus (E) [GPa] versus Poisson's ratio (ν) for intact (non-reacted) BB and TR sandstone core samples. The subplots are color-coded with experimental confining pressure [MPa] and test temperature [°C]. Figures SI-1/2 demonstrates laboratory E and ν values plotted for BB and TR individual specimens separately against changes in stress and temperature test conditions (refer to Supplementary Information).

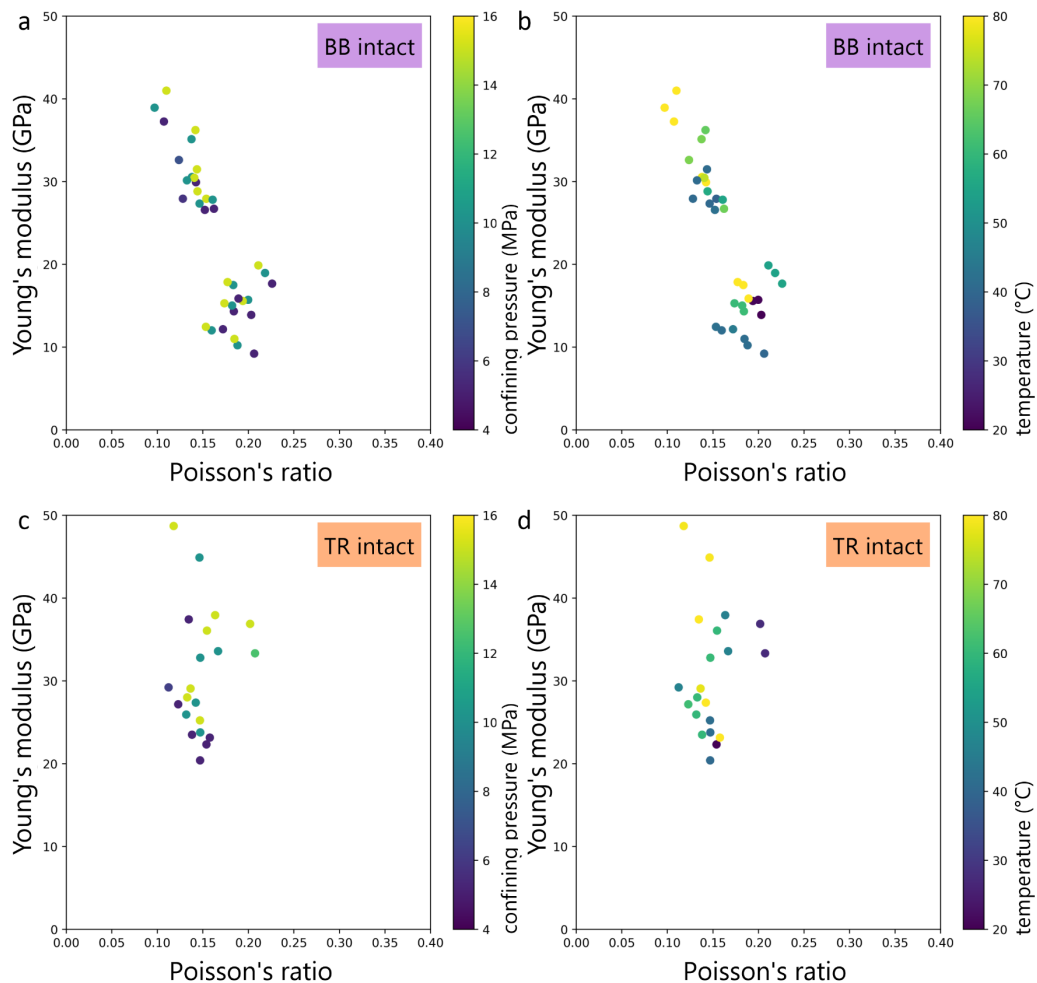


Figure 3. Crossplots of Young's modulus (E) [GPa] versus Poisson's ratio (ν) for intact (non-reacted) (top) Boise Buff (BB) and (bottom) Torrey Red (TR) porous sandstones. The subplots are color-coded with (a, c) experimental confining pressure [MPa] and (b, d) test temperature [°C].

Subfigures 3a-b reveal that the triaxial compression tests characterized two subgroups of intact BB sandstones, indicating natural heterogeneities within the layered porous rocks. Group A shows $E=26-41$ GPa and $\nu=0.09-0.17$, while the group B was characterized with $E=9-21$ GPa and $\nu=0.15-0.24$. An increase in confining pressure (P_c) from 5 to 15 MPa during the experiments resulted in increase in Young's modulus for both subgroups (Fig. SI-1/2). An increase in the experimental temperature (T), ranging from 20-80 °C, resulted in increase in the elastic modulus (higher E values) (Figs. 3b and SI-2b). The increase in P_c caused a slight decrease in Poisson's ratio of both subgroups but the impact of temperature variations in Poisson's ratio is indistinct (Fig. SI-1/2).

Similarly, the elastic moduli of TR sandstones suggest two subgroups but with a smaller gap between the measured values (Figs. 3c-d). The E - ν ranges are as follows: In subgroup A, $E=18-29$ GPa and $\nu=0.11-0.16$, and in group B, $E=32-49$ GPa and $\nu=0.12-0.22$. The impact of an increase in P_c and T on E - ν values of TR core samples are similar to BB, particularly for subgroup B (Fig. SI-1/2e-h).

As confining pressure rises, the rock undergoes a more even stress distribution, concurrently experiencing a reduction in deformability. This phenomenon is attributed to the increased confining pressure diminishing void spaces within the rock, rendering it less susceptible to deformations. Consequently, porous sandstones exhibit greater stiffness, exemplified by the observed increase in Young's modulus at elevated confining pressures of Figure 3. The elevation in confining pressure induces a reduction in pore spaces within the rock, emphasizing a direct link between increased confining pressure and enhanced mechanical integrity.

The influence of confining pressure extends to Poisson's ratio, primarily through its impact on the lateral contraction of the rock. The higher confining pressure effectively constrains lateral deformation, manifesting in a consequential decrease in Poisson's ratio. This observed decrease in Poisson's ratio bears significance, providing insights into how the mechanical behavior of the rock dynamically responds to varying stress conditions (Fig. 3). These interrelated effects collectively contribute to the intricate relationship between confining pressure, pore structure, and the mechanical properties of porous sandstones.

The influence of temperature involves a combination of effects, including thermal expansion of minerals and potential enhancement of grain-to-grain contact, among others. As temperatures elevate, individual mineral grains within the sandstone undergo thermal expansion, fostering a tighter packing that translates into a notable increase in stiffness or modulus. This thermal rise not only influences the physical dimensions of the mineral constituents but also fosters enhanced cohesion between grains, culminating in a rock matrix characterized by greater stiffness and reduced deformability.

It's crucial to acknowledge the nuanced nature of Young's modulus behavior with temperature in porous sandstones. The complexity arises from diverse factors, including mineral composition, porosity, cementation, and fluid type, each contributing to the material-specific interplay of these influences. The literature underscores multifaceted understanding of these interdependent factors, emphasizing their role in shaping the thermal response of porous sandstones (Orlander et al., 2021; Ranjith et al., 2012; Sun et al., 2016; Wang et al., 2022).

3.3.2. Deformation of acid-treated sandstones

The results of rock mechanical tests of BB and TR sandstones after treatment with CO₂-acidified brine (10 MPa fluid pressure and 60 °C for 7 days) are presented in Figures 4 and SI-3/4. The CO₂-reacted BB and TR sandstones show E moduli of 17-28 and 21-34 GPa, respectively. The ν ranges 0.13-0.23 and 0.18-0.33 for BB and TR. Therefore, the measured Poisson's ratio of these two sandstone sets are slightly higher than the non-reacted (intact) core samples, particularly evident for TR samples. For the tested BB and TR sandstones, the elastic modulus (E) systematically increases as the experimental temperature and confining pressure increase (Figs. 4 and SI-3/4). Increase in T resulted in an increase of ν in BB specimens, but a decrease in TR porous rocks (Figs., 4b,d and SI-4d,h). As Figure SI-4 shows, changes in the experimental stress regime (i.e., confining pressure) correspond with a minor increase in E and ν BBs but more pronounced growth in TRs.

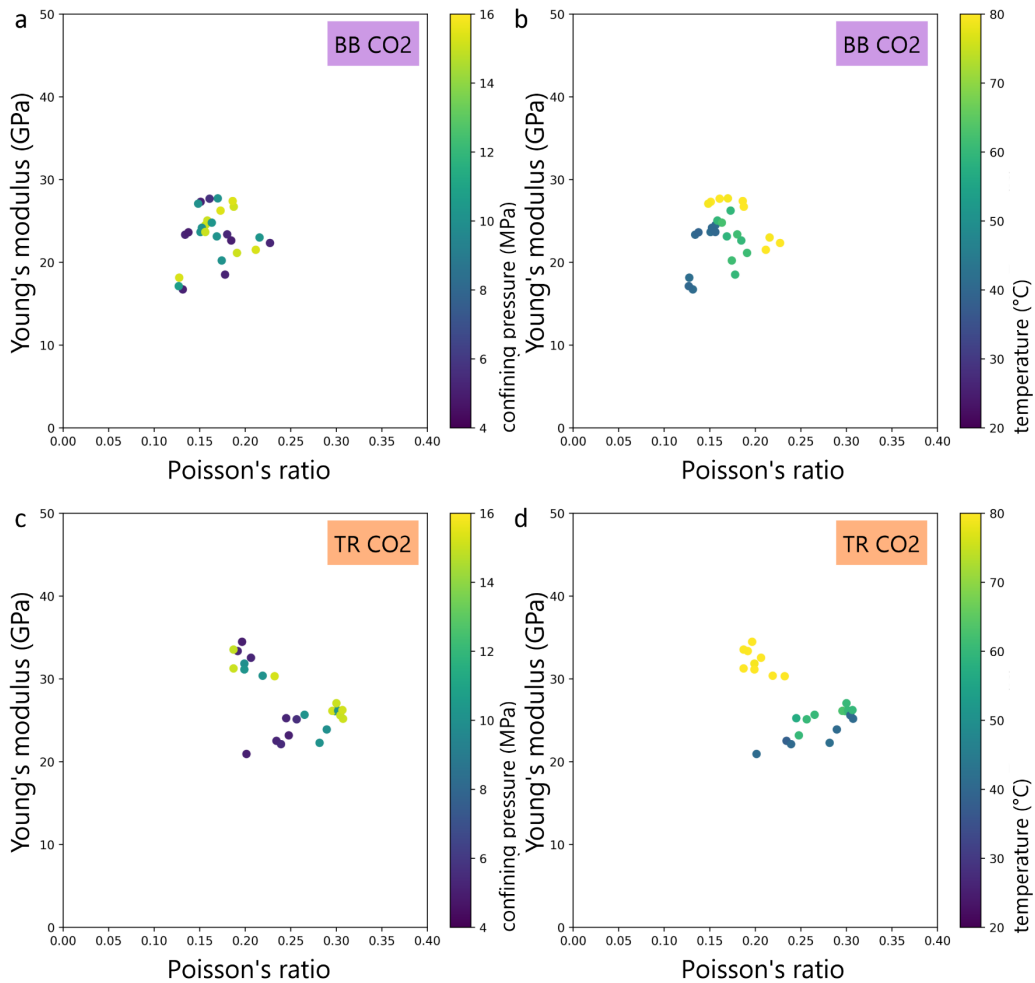


Figure 4. Crossplots of Young's modulus (E) [GPa] versus Poisson's ratio (ν) of (top) Boise Buff (BB) and (bottom) Torrey Red (TR) sandstones after treatment with CO₂-acidified brine. The subplots are color-coded with (a, c) experimental confining pressure [MPa] and (b, d) test temperature [°C].

The acidification of the brine, facilitated by continuous supply of ScCO₂, may have initiated subtle adjustments within the sandstone grain contacts and porous matrix, influencing rock microstructure and grain contacts without entailing any rapid or major mineralogical transformations. Concurrently, the treatment might have subtly influenced the pore structure of the rock, impacting the elastic modulus and Poisson's ratio of the sandstone. The observed elevation in elastic modulus with experimental temperature and confining pressure implies the influence of these external factors on the sandstone's mechanical response. The varied responses in TR and BB sandstones likely stem from

differences in their initial mineralogical composition, cementation and fines, and pore volume compliance, resulting in distinctive changes. These findings provide insights into the effects of acidified brine and clean reservoir sandstone, shedding light on the complex mechanical behavior of CO₂ storage reservoir rocks. For a more in-depth exploration, we direct the reader to Table 1 (see appendix) and the detailed literature review presented in the introduction, providing an overview of chemo-mechanical interactions and range of variations in geomechanical properties in these conditions.

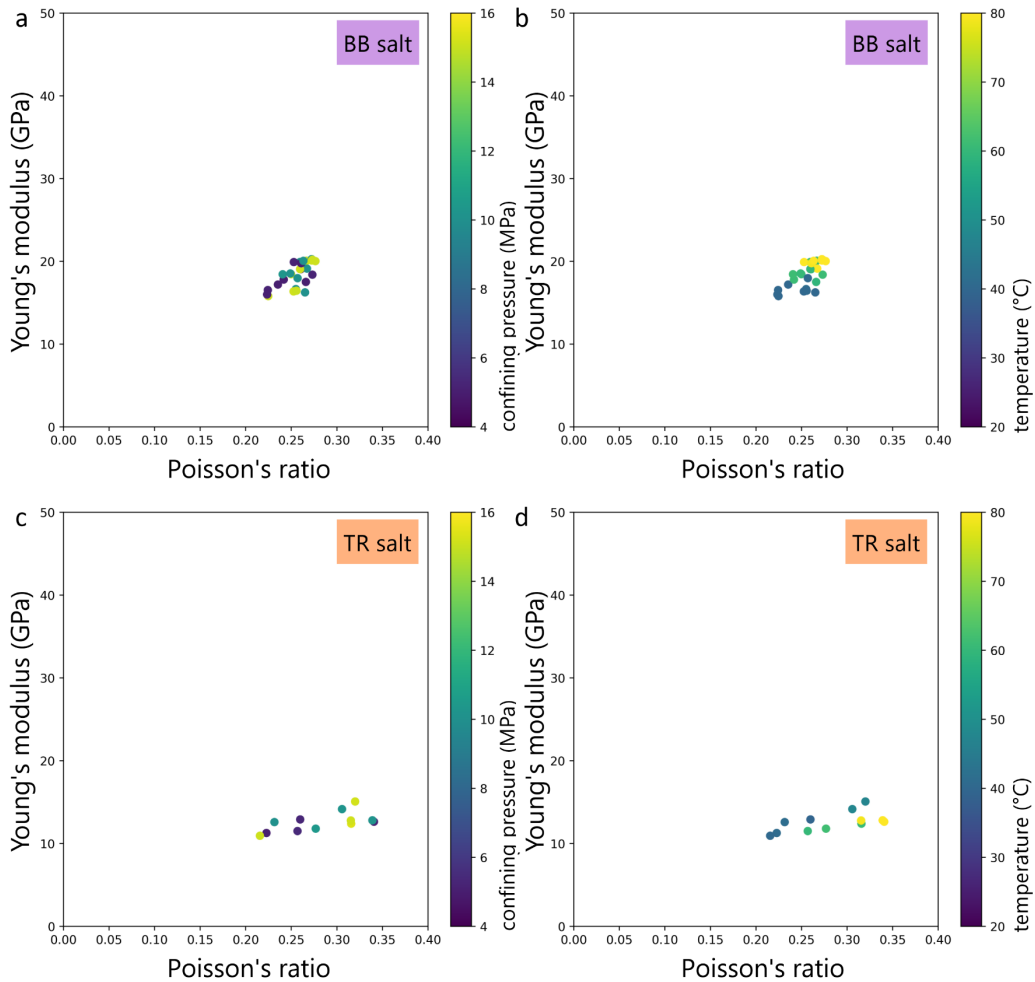


Figure 5. Crossplots of Young's modulus (E) [GPa] versus Poisson's ratio (ν) of (top) Boise Buff (BB) and (bottom) Torrey Red (TR) sandstones affected by CO₂-induced salt precipitation. The subplots are color-coded with (a, c) experimental confining pressure [MPa] and (b, d) test temperature [°C].

3.3.3. Deformation of crystallization-affected sandstones

Figures 5 and SI-5/6 show the elastic parameters of sandstones affected by CO₂-induced salt crystallization. A marked reduction in Young's modulus is evident in both BB and TR sandstones, with Young's modulus ranging from 15-21 GPa for BB and 10-15 GPa for TR core samples. These values represent approximately half of the average values measured for intact and CO₂-reacted specimens, underscoring the substantial impact of salt crystallization on the mechanical properties. The TR core samples, characterized by tighter properties such as lower porosity and significantly reduced permeability, exhibit a more pronounced decline in elastic moduli compared to BBs. This observation suggests that the initial characteristics of the sandstone play a crucial role in determining the extent of mechanical degradation induced by salt crystallization. The measured Poisson's ratios show a noteworthy increase of approximately 1.5 compared to previous cases, covering a range of 0.22-0.29 for BB and 0.21-0.34 for TR sandstones. Subplots in Figures SI-5/6 reveal that the increase in confining

pressure and test temperature during the experiments leads to an elevation in both E and ν parameters, the slope of which might seem gentler than previous cases.

It is worth mentioning, one of the TR core samples were damaged rapidly and intensively during the initiation phase of the experiments with salt-damaged TRs, indicating a dramatic decline in the strength parameters after the salt crystallization in porous media and continued growth. That is the reason why Figure SI-6 includes only two plotted samples.

3.4. Mechanical parameters deterioration

Figure 6 juxtaposes Young's and shear moduli of intact, treated with CO_2 -acidified brine, and salt crystallization-damaged BB and TR sandstones as a function of increased confining pressure. It shows how the mechanical properties of these three sets of experiments were affected as stress regimes and geochemical factors varied.

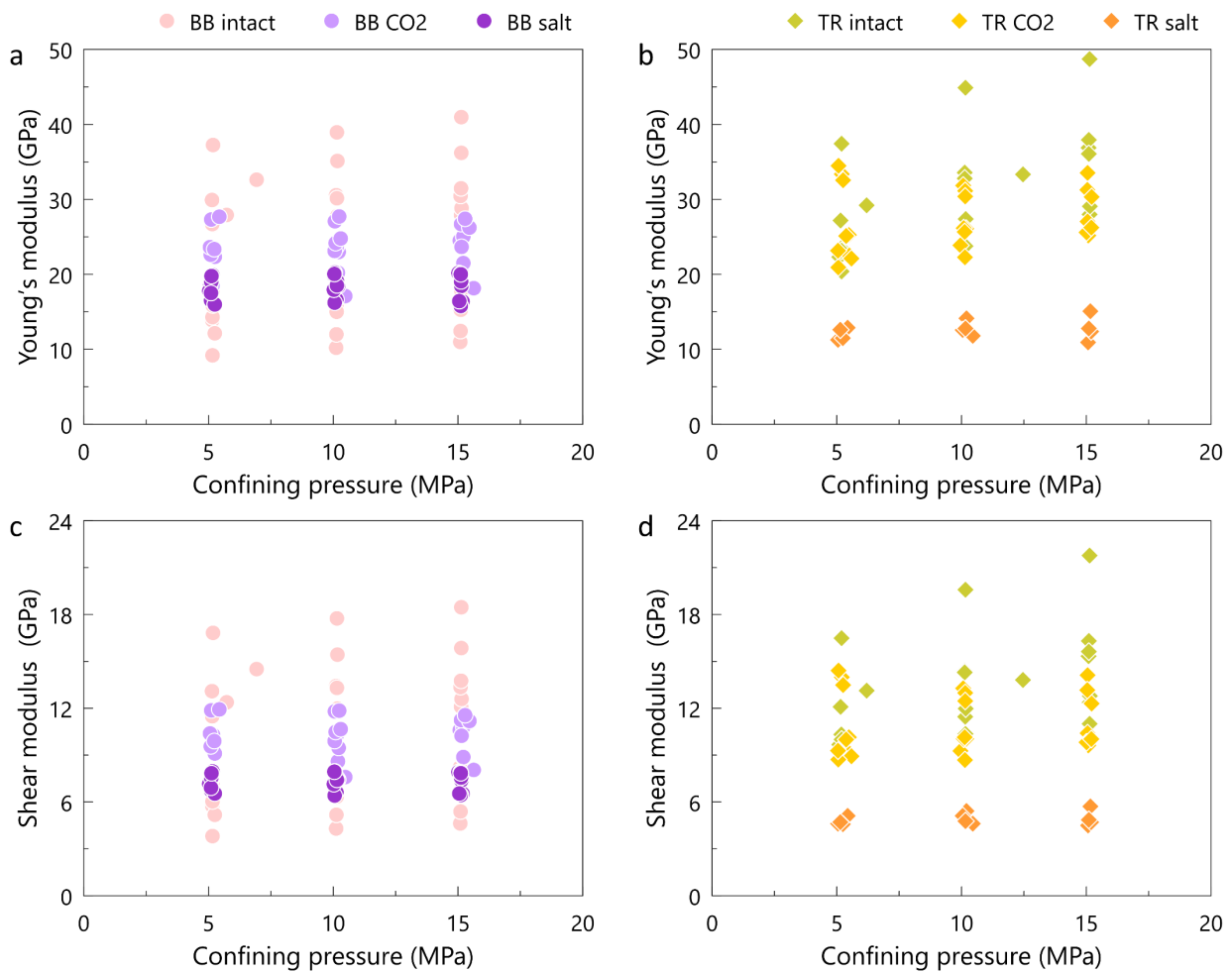


Figure 6. Stress sensitivity of (a, c) Young's [GPa] and (b, d) shear moduli [GPa] of intact, CO_2 -acidified brine-treated, and salt crystallization-damaged (left) Boise Buff (BB) and (right) Torrey Red (TR) sandstones as a function of increase in confining pressure [MPa]. The subplots illustrate the impact on the mechanical properties of these three sets of experiments, showcasing variations in stress regimes and geochemical factors.

As Figure 6 illustrates for tested subgroups of BB and TR rocks, the mechanical properties of a given sandstone rock type are intricately shaped by a myriad of natural heterogeneities, encompassing variations in pore volume, grain framework, mineral composition, grain contacts, and cementation, among others. The inherent heterogeneity, rooted in complex sedimentation processes, manifests as

discernible differences in grain size, sorting, and layering within the rock. Simultaneously, the mineralogical composition, incorporating minerals such as quartz, feldspar, and clay, introduces an additional layer of complexity to the sandstone's mechanical behavior. Rock properties are then subsequently controlled by the degree of mechanical and chemical compactions and burial history (Bjørlykke, 2015; Bjørlykke and Jahren, 2015; Nooraiepour, 2022, 2019, 2018), reflected in present-day porosity-permeability profile of these two reservoir quality classes (refer to Section 3.1).

These compositional variations play a pivotal role in determining the elastic moduli (and predictive modeling of long-term subsurface coupled THMC processes), encompassing parameters like Young's modulus and shear modulus, as well as influencing strength parameters such as compressive and tensile strength. Additionally, these variations govern the rock's deformation behavior, contributing to localized differences in brittleness and ductility. Anisotropy, stemming from grain orientation, imparts directional dependence to the mechanical properties, further enriching the understanding of the sandstones' response to applied stress.

By juxtaposing datapoints in Figure 6, two discernible trends emerge, each contributing to a deeper understanding of the mechanical behavior of sandstone classes (BB or TR). Firstly, as defined by inherent heterogeneities, the initial variation domains depict distinct differences between the two classes, with BB exhibiting a broader scatter than TR, as also illustrated in Figure 3. It is essential to emphasize that each class is characterized by a range of properties rather than a single estimator. However, as we transition from intact to CO₂-treated and salt-damaged rocks, the degree of variation across the ordinate (*y*-axis representing moduli) diminishes.

Secondly, the deterioration of Young's and shear moduli due to CO₂-induced salt crystallization damage is notable. While each experimental subsets indicate the expected trend as confining experiments is increased in triaxial experiments (in addition to temperature change), a systematic decline is observable. While this impact is not distinct enough due to the wide spread of intact BB specimens, the marked strength reduction of TRs to approximately half is demonstrated in Figs. 6b,d. The post-interaction TR specimens, affected by salt crystallization damage, vividly portray a potential upper-band mechanical weakening, clearly depicting the deleterious effects of salt-induced alterations on the sandstone's mechanical integrity. We posit that the observed decline represents the upper limit of damage, manifested through the continuation to complete dry-out and extensive precipitation at our experimental conditions. Notably, our experimental observations align with findings documenting such a decline in dynamic elastic parameters, as computed using measured compressional and shear wave velocities (Zhang et al., 2020).

The tighter TR rocks (with lower reservoir quality) demonstrate higher Young's and shear moduli in addition to the higher peak strength compared to more porous-permeable BB specimens (with higher reservoir quality). However, salt crystallization and crystal growth inside the porous sandstone geometries damaged the TR sandstones more intensively than the BBs, leading to more aggressive mechanical weakening (Fig. 6d). Computed shear moduli show a decrease from a maximum of 22 and 18 GPa for intact sandstones to 6-8 and 4-6 GPa for salt-damaged TR and BB rocks, respectively (Fig. 6). As an average, the decrease for BBs is to half and for TRs to a third. The CO₂-reacted specimens show μ values between these two extremes. The significant reduction in rigidity observed here indicates an increased susceptibility to shear failure. This may occur as a potential risk

when the in-situ shear stress surpasses the shear strength of CO₂ storage reservoirs, particularly in the near-wellbore regions.

To evaluate the brittleness and ductility of the intact and reacted sandstones, we constructed crossplots of Young's modulus versus Poisson's ratio and shear modulus or rigidity (μ) versus incompressibility (λ) in Figure 7. Figure 7b is a modification of the well-known λ - μ rock physics crossplot, where the bulk density (ρ) is factored out. The classification of regions is adopted from review of literature on brightness-ductility classifications presented in Nooraiepour et al. (2017). Figure SI-7 shows Lamé's first and second parameters (λ - μ) plots for different experimental cases separately.

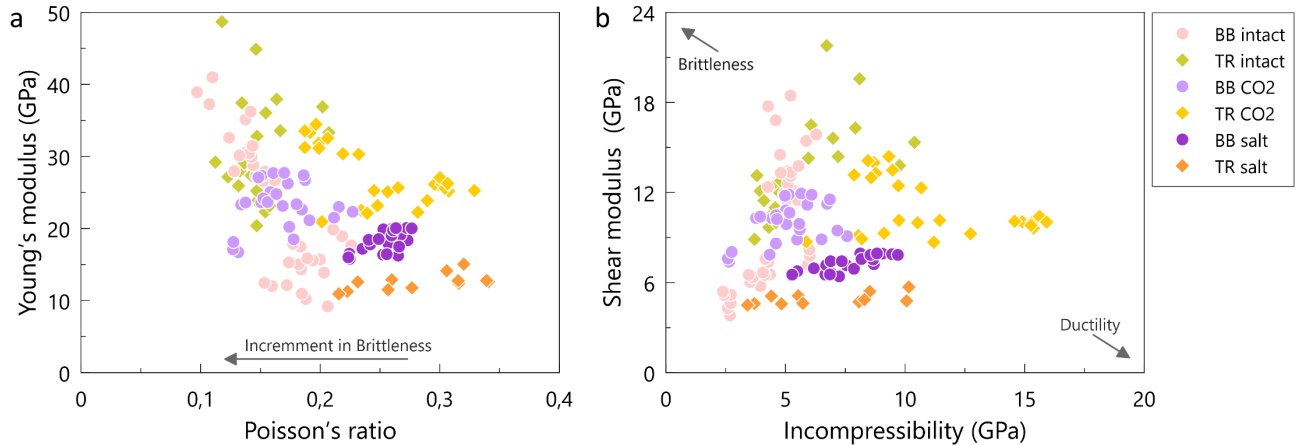


Figure 7. Rock physics crossplots evaluating brittleness and ductility of intact and reacted sandstones: (a) Young's modulus vs. Poisson's ratio, and (b) shear modulus vs. incompressibility. Subplot b is modified from λ - μ crossplot, where bulk density (ρ) is factored out. Regional classification follows the literature review on brightness-ductility presented in Nooraiepour et al. (2017).

Comparison between Figs. 7a-b demonstrates that different proxies for brittleness evaluation can provide slightly different assessment results. Overall, Figure 7 suggests that the treatment of samples caused a shift in the geomechanical properties of BB and TR sandstones toward the more ductile regions. In both subplots, to a large extent, a movement of data points toward the bottom right is evident, particularly for the E- ν crossplot (Fig. 7a), when one juxtaposes static rock mechanical parameters of intact, CO₂-reacted and salt-affected porous rocks. However, the λ - μ relationship of tested specimens does not necessarily suggest that reacted BB and TR show markedly increased ductility (Fig. 7b).

4. Salt crystallization damage in the carbon sequestration context

4.1. Mechanical weakening of saline aquifers

As presented in Table 1 (see the appendix), laboratory investigations to comprehend the interactions between CO₂, brine (water), and rock constituents have provided extensive insights into relatively short-term geochemical consequences, typically spanning a maximum of 2-3 years. However, there still exists a knowledge gap concerning the protracted reaction mechanisms and combined consequences when the contribution of quick carbonate (calcite) mineral dissolution is minuscule, particularly in clean reservoir sandstones. Experiences from industrial and pilot CCS projects worldwide have undoubtedly built solid scientific and operational grounds. However, laboratory and numerical efforts have repeatedly shown the necessity of further thorough investigation of physico-chemical processes with potential coupled THMC challenges for scale-up.

It has been shown that CO₂-brine-rock interactions are ubiquitous in carbon storage reservoirs with the potential for triggering mechanical damage in sandstone rocks. These mechanical damages primarily result from physical changes in the rock microstructure due to fluid-rock reactions/interactions through mechanisms such as mineral alteration/transformation, clay swelling and shrinking, pressure buildup in pores, redistribution of fines, thermal stress, and local stress concentration within porous geometries (Table 1).

We expect the highest probability of (geo)chemically induced mechanical damages to occur in the near wellbore environment where the highest acidity (lowest pH) of formation water is achieved due to carbon dioxide dissolution and carbonic acid generation. This region also endures the fastest CO₂ flow through the pore volume, highest viscous forces, potentially highest pressure buildup, lowest chemical buffering of reactive pore fluid, and most significant thermal stresses. Additionally, CO₂-induced salt precipitation may substantially threaten the mechanical integrity of near injection well zones.

The study of salt crystallization has seen a dynamic convergence of various scientific disciplines to unravel the microscopic underpinnings of processes governing salt precipitation dynamics, salt weathering mechanisms, and consequent damages. An expression to calculate the crystallization pressure as a function of the supersaturation was first derived by Correns and Steinborn (Correns and Steinborn, 1939, translated and commented upon by Flatt et al., 2007). Everett (Everett, 1961) pursued an alternative method to address the issue, establishing a connection between crystallization pressure and the characteristics of curved interfaces existing between crystals and their respective solutions. In the last two decades, consensus has been reached that salt precipitation and growth under confined and supersaturated conditions exert crystallization pressure.

The prevailing theory posits that crystallization pressure within pores arises from a thermodynamic interaction resulting from a non-equilibrium state created by solution supersaturation (Flatt, 2002; Flatt et al., 2007; Scherer, 2004; Steiger, 2005a), and interfacial energies as repulsive disjoining force operating between the pore wall and the burgeoning crystal (when there is a liquid film between the crystal and the confining surface) (Coussy, 2006; Espinosa-Marzal and Scherer, 2010; Hamilton et al., 2010; Scherer, 2004; Steiger, 2005b). A formulation for crystallization pressure, harmonizing with both models, was subsequently devised, which incorporates Pitzer's (Pitzer, 1991) ion interaction approach to account for the nonideal behavior of the liquid phase, ensuring comprehensive consideration (Flatt et al., 2017; Flatt, 2002; Steiger, 2005a, 2005b). The theoretical formulations signify the maximum pressure applied to a pore wall, achievable only at equilibrium when a sizable crystal is confined within a pore with narrow throats. It also marks the highest transient pressure exerted when a crystal growing in a large pore initially encounters the wall. As the crystal expands, it diminishes the local supersaturation, leading to a subsequent decrease in pressure (Flatt et al., 2017) under the assumption that crystal growth consumes the solutes faster than its transport to the sites by mechanisms such as diffusion, capillary backflow, and water film flow across grain surfaces.

The growing crystal experiences distinct pressures on its various faces. Faces in contact with the liquid solution undergo the pressure of the pore solution, whereas those in contact with the confining surface via the liquid film are presumed to experience crystal pressure. The existence of this disjoining

force is attributed to the fact that the energy associated with the salt or mineral interface, which would form when the crystal grows adjacent to the pore wall, exceeds the cumulative energies of the salt-to-solution and mineral-to-solution interfaces (Espinosa-Marzal and Scherer, 2010; Flatt et al., 2017). The crystal pressure is determined to be higher than that of the surrounding solution, as indicated by Scherer et al. (2001) and Steiger (2005a,b). Therefore, the salt crystallization pressure will apply as crystals form within their porous hosts, placing the hosts under tensile stresses (Derluyn et al., 2014; Flatt et al., 2014). These forces can harm materials like reservoir rocks with relatively low tensile strength.

Steiger (2005a) computed (maximum) crystallization pressure (using Eq. 19 in his paper) in supersaturated solutions containing aqueous NaCl, NaNO₃, Na₂SO₄, and MgSO₄, commonly found in natural rock environments. The calculations incorporated both the anhydrous and hydrous phases of these salts. The results demonstrated that the crystallization pressures generated at low to moderate supersaturation levels are capable of inducing tensile stresses on the pore walls. Notably, these stresses surpass the tensile strength of many saline aquifer reservoir rocks. For instance, at supersaturation levels of 1.2, all the salts, except mirabilite, exhibited significantly higher crystallization pressures than the tensile strength of sandstone (assuming approximate average of 3-4 MPa) (Shao et al., 2022; Steiger, 2005a).

The significance of thin liquid films in crystallization pressure has already been highlighted in theory (Desarnaud et al., 2016; Espinosa-Marzal and Scherer, 2010). To generate crystallization pressure, upholding a liquid film through repulsive forces acting between the crystal and the wall is imperative to facilitate the ongoing growth of the crystal by incorporating additional ions into its lattice. It is crucial to note that if a growing crystal completely spans the void between two enclosing walls, no crystallization pressure can emerge, as there is no opportunity to add extra salt layers and create such pressure. It has been shown (experimentally and numerically) that salt crystals can draw water from neighboring mineral grains by establishing persistent water films covering/wetting mineral grains (Masoudi et al., 2023; Miri et al., 2015; Nooraiepour et al., 2018; Nooraiepour et al., 2019; Ott et al., 2021; Qazi et al., 2019), primarily due to surface energy influences. Consequently, a perpetually replenished brine source is made available to sustain the advancing evaporation front, ensuring a consistent expansion of salt crystals upon pre-existing salt aggregates. The water films may exhibit notable mobility and conductivity for solute transport. The significance of the presence of water film was studied using hydrophilic and hydrophobic glass plates (Desarnaud et al., 2016). Hydrophobic glasses, which impede the formation of a wetting film, did not register any pressure. In contrast, hydrophilic glass slides facilitated the formation of a thin film, resulting in a significant crystallization pressure. The crystallization pressure for halite (NaCl) and sylvite (KCl) increased with higher salt concentrations, aligning with theoretical expectations. For a given salt concentration, halite exhibited markedly higher crystallization pressure (Desarnaud et al., 2016).

4.2. Conceptual model of microscale crystallization damage

Figure 8 provides scanning electron microscopy (SEM) of microscale adverse effects of salt crystallization in reservoir sandstones. We use these direct observations, describe them below, and in Figure 9 propose a series of conceptual damage mechanisms induced by CO₂-induced salt precipitation. We limit the presentation of direct imaging evidence to SEM micrographs in this paper, avoiding micro-CT segmented images to prevent unwarranted speculation and biased interpretations.

The imaging specifications hinder the detection of cracks and fissures in individual matrix grains of brittle quartz and feldspar mineral grains. Our exploration of the Digital Rock Portal reveals that only high-resolution (super-resolution) tomography can partially capture certain features illustrated in Figure 8 and conceptualized in Figure 9.

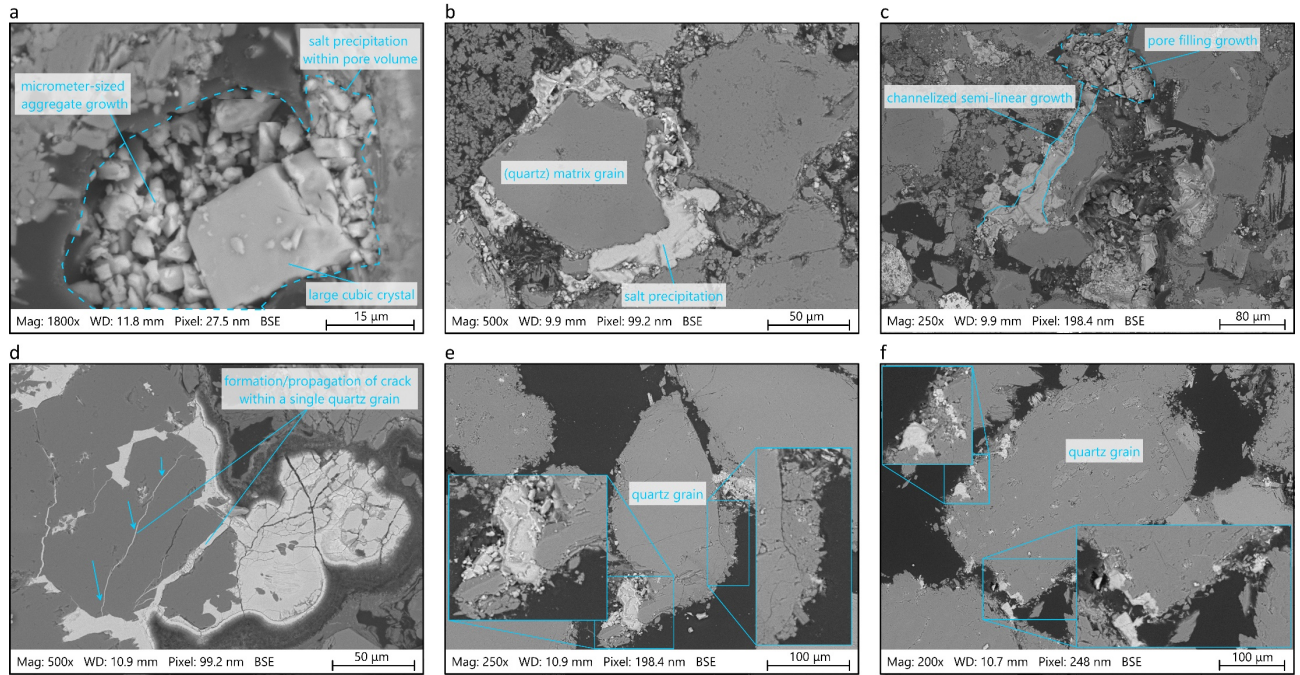


Figure 8. Scanning electron microscopy (SEM) images showcasing salt crystallization effects on sandstones: (a) salt precipitation and continuous growth in a pore body, featuring a large cubic crystal and micrometer-sized aggregated growth; (b) salt precipitation occupying throats between matrix grains and partially filling pore volumes around a quartz grain; (c) channelized semi-linear salt growth along several grains connected to a nearly complete clogged pore volume; (d) crystallization of salt bodies within cracks inside the quartz grain, with potential for evolution into significant fractures of varying sizes; (e-f) a quartz grain displaying topological damage features such as chipping and abrasion due to peripheral salt nucleation and growth.

Despite the limitations in spatial resolution of our tomography, conducted x-ray imaging on postreaction specimens successfully identified certain larger-scale conceptualized mechanisms. Notably, we observed dilations in various regions of the porous media. Considering the limited geochemical reactivity of our clean BB and TR sandstones, we interpret the expansion of samples as a consequence of localized volumetric increases induced by salt precipitation and growth (similarly reported also by Falcon-Suarez et al., 2020). If our ongoing investigation confirms the observation of rock frame dilation due to CO₂-induced salt precipitation in sandstones with high porosity-permeability and low reactivity to CO₂, then early detection of salt precipitation near the wellbore region becomes imperative. This is crucial for preserving both the injectivity properties of the reservoir and its mechanical integrity.

Upon initiating CO₂ injection, a distinct two-phase-flow zone emerges, featuring an aqueous phase alongside a CO₂-rich phase (Fig. 9a). This process, known as two-phase displacement, is primarily characterized by viscous displacement sweeping brine from around the injection well. As the flooding front, representing a shock front, progresses it leaves behind a zone where residual brine is confined in diverse configurations, such as thin wetting films enveloping grain surfaces and liquid bridges or pools within pores. This drained region faces a continuous flow of dry scCO₂ with low water vapor pressure, initiating an evaporation regime. Persistent flow leads to substantial water evaporation

into the CO₂ stream, inducing dry-out. While both two-phase displacement and evaporation contribute to water removal near the well, the time scales of these processes remain distinct.

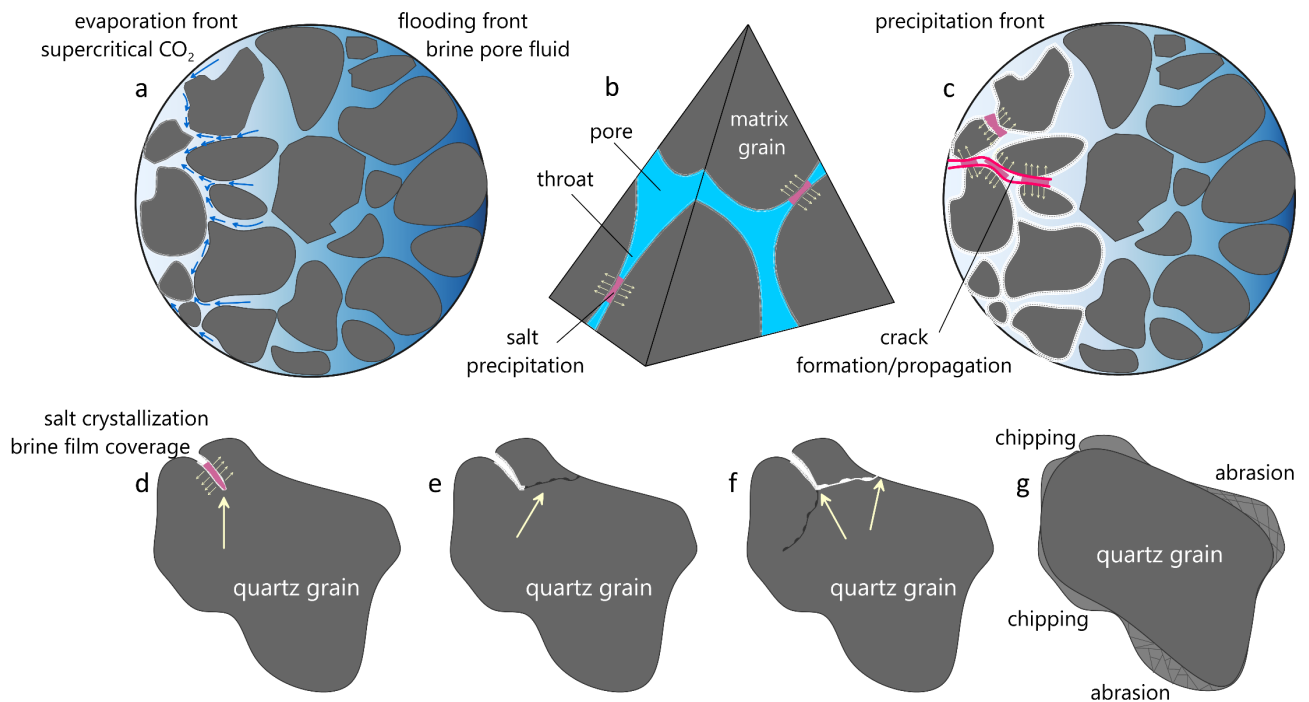


Figure 9. A schematic representation elucidating microscale mechanisms involved in salt crystallization damage in porous rocks. (a) depiction of evaporation front formation, flooding front, initiation of salt nucleation and growth, and capillary-driven backflow of water films. (b) salt crystal growth along grain surfaces, within the throats, and inside the pore bodies, exerting significant internal stresses on the surrounding matrix grains or porous medium's structure. (c) initial fissures, whether induced in the previous step or naturally occurring in the rock framework, are filled with brine, subject to nucleation and growth, and exposed to crystallization damage. This sequence of events extends to brittle sandstone grains with natural defects and initial cracks formed during transport and diagenesis (mechanical compaction). (d) fracture extension occurs at existing cracks within or around the edges of brittle grain matrix due to migrating water films and crystallization-induced mechanical stress. (e-f) additional cracks are initiated through further nucleation and precipitation events on a secondary substrate (previously crystallized salts), ultimately resulting in extensive fracturing and breakdown of the quartz grain. (g) nucleation and growth of salt crystals may also trigger topological grain damages such as chipping and abrasion.

The primary water mass exchange occurs in the dry-out zone, generating a saturation gradient across the drying front significantly greater than that in a pure viscous displacement. This gradient, driven by capillary pressure, drives water towards the evaporation front, intensifying evaporation (blue arrows in Fig. 9a). Additionally, as water evaporates into the CO₂ stream, increasing salt concentration in trapped brine leads to outward salt diffusion from the drying front. The distance between the dry-out and flooding fronts is primarily regulated by capillary backflow and solute diffusion. Once salt concentration reaches its solubility limit due to evaporation, salt precipitates, exhibiting a strong affinity for brine and facilitating further precipitation (Figs. 8-9/b-c). Salt-induced capillary backflow enhances the stability of water films, augmenting continued accelerated salt precipitation (Miri and Hellevang, 2016).

Continuous (repetitive) wetting-drying cycles, driven by capillary suction and continuous brine films supply in pore volumes, lead to crystal growth along grain surfaces, throats, and pore bodies (Figs. 8-9/b-c). As the salts crystallize inside the porous medium, they undergo a change in physical state from a dissolved solute to a solid crystal lattice, and crystallization pressures are built up. This induces considerable internal stresses on the surrounding matrix grains or porous medium's structure (Figs. 8-

9/b-c). The internal stresses generated by salt crystallization can reach a point where they exceed the material's tensile strength. The tendency for crystals to preferentially grow in narrow pore throats (Miri et al., 2015) significantly influences the sandstone's internal geometric structure evolution, with narrow throats being particularly susceptible to salt damage (Figs. 8-9b).

Initial fissures, whether induced or naturally occurring, are filled with brine and exposed to crystallization damage. As crystals grow during drying, they exert substantial crystallization pressure on fissure walls, causing cracks (Figs. 8-9c). Small microcracks may initiate within the material, typically at weak points or grain boundaries that mark the crack initiation stage. The continued crystallization and growth lead to stress accumulation, during which these microcracks can propagate further into the material, extending and deepening the damage (Figs. 8-9c). During crack propagation, small pores are preferentially cracked and connected. If the in-situ stress continues to build, the precipitation-induced/enhanced cracks may have the potential to evolve into more significant fractures (with various sizes). These micro- to macro-scale deterioration chain of events in material properties may sum up to colossal weakening of the solid and porous structure.

It should be noted that different salt solutions exhibit distinct crystallization characteristics, leading to varying degrees of rock deterioration (ongoing study). Thus, further research is recommended to explore the impact of different salt solutions on rock deterioration, focusing on crystal growth features.

Quartz and feldspar, as prevalent constituents of sandstone, exhibit pronounced brittle characteristics owing to their mineral structure and mechanical properties. The crystalline structure of quartz, comprising tightly packed silicon dioxide units, renders it susceptible to fracture and breakage under applied stress, particularly in the presence of mechanical discontinuities or stress concentrations. Similarly, feldspar, a framework aluminosilicate mineral, exhibits brittleness due to its complex lattice structure and susceptibility to cleavage along specific crystallographic planes. The brittle nature of quartz and feldspar influences the overall mechanical behavior of sandstone, contributing to fracture initiation, propagation, and the overall deformation response of the rock under varying stress conditions.

Figures 9d-f present a schematic illustration of a potential mechanical deterioration mechanism focusing on the disintegration process of quartz grains. This representation is derived from a meticulous examination using high-resolution SEM of BB and TR samples at the matrix grain scale, as depicted in Figures 8d-f. Building upon the earlier-discussed chain of events responsible for pore-scale mechanical damages, we extend the implications to brittle sandstone grains characterized by natural defects and initial cracks formed during transport and diagenesis.

Theoretically, water-filled pore bodies induce internal strain through volume expansion and mechanical stress during salt growth. These stress factors are initiated at point defects and vary in intensity based on the presence of inclusion trails. Fracture extension occurs at existing fractures from inclusion trails and subgrain boundaries due to migrating water and crystallization-induced mechanical stress (Fig. 9d). Additional fractures are initiated through further nucleation and precipitation events on a secondary substrate (previously crystallized salts) (Masoudi et al., 2022; Nooraiepour et al., 2021a) (Figs. 8c, 9e). Ultimately, extensive fracturing leads to the breakdown of the quartz grain (Figs. 8c, 9f).

Repetitive observations in SEM micrographs suggest that particles with topographical features or angular surfaces may undergo chipping breakage, where the application of load on an irregular particle result in the breakage of rough corners (Fig. 8e). This chipping phenomenon occurs when edges or corners of a particle break off. Additionally, attrition loading can induce abrasion, which occurs when the applied energy is insufficient to cause significant particle breakage. Abrasion is also characterized by the generation of fines around matrix grains with no noticeable change in the mean diameter of the feed particle (Fig. 8f).

Juxtaposing the results of two reservoir sandstone classes in this study clearly indicates that the significance of pore size (distribution) in the damage resulting from salt subflorescence (i.e., precipitation and growth inside the porous material) cannot be overstated. It profoundly impacts the crystallization pressure and the distribution of minerals (Derluyn et al., 2014; Nadelman and Kurtis, 2019; Shokri-Kuehni et al., 2018; Yu and Oguchi, 2010). In reservoir rocks characterized by smaller pores, the crystallization pressure is notably higher than in layers with larger pores, and precipitation occurs deeper inside the evaporation front. These two factors collectively contribute to increased deterioration and reduced mechanical strength to subsequent salt crystallization. And finally, salt crystallization is a cyclic process (Balboni et al., 2011; Desarnaud et al., 2013). Each wetting and drying cycle leads to additional salt crystallization, causing further expansion, stress, and damage. The cumulative effect can be substantial, particularly in structures and geological formations exposed to these cycles for extended periods.

5. Conclusions

New laboratory experiments provide crucial insights into the geomechanical response of two distinct sandstone reservoirs, Boise Buff (BB) and Torrey Red (TR), under varying geological and geochemical conditions. BB and TR sandstones exhibit notable variations in their sedimentary characteristics. BB sandstone represents better reservoir quality with coarser matrix grains, lower cementation, larger intergranular porosity, and improved pore connectivity, rendering it highly permeable. Conversely, TR sandstones feature finer matrix grains, tighter pore space, and narrower throat sizes but have greater mechanical strength. The main findings can be succinctly outlined as follows:

- Analysis of existing research reveals that the rapid reaction rate of calcium carbonates can explain the interactions of CO₂ and carbonic acid with reservoir sandstones containing calcite. However, certain sandstone reservoirs lacking fast-reacting minerals exhibit a decline in mechanical properties when exposed to CO₂ and CO₂-acidified brine. While some studies attribute this to alterations in grain-to-grain contact points, others merely report the observed changes. Concluding our research, we highlight an existing knowledge gap in this domain, underscoring the need for additional targeted studies to explicitly explain potential microscale alterations. It is imperative to delve into the mechanisms and specific governing factors, supported by microscale evidence, that elucidate conditions when geochemical reactions resulting in composition changes are absent, yet significant mechanical consequences are observable in clean reservoir aquifers.
- Stress-Strain Relationships: Triaxial compression tests reveal that TR sandstones exhibit nearly double the peak strength of BB samples. BB porous rocks reach yield strength at lower strains and exhibit a more confined plastic deformation region. In contrast, TR sandstones display

higher mechanical strength, a stiffer characteristic, and a more extensive plastic deformation range.

- Geomechanical Alterations: CO₂-brine-rock interactions emerge as a critical factor affecting the rock mechanical properties of sandstones. The study demonstrates how changes in confining pressure and temperature affect the elastic properties of both sandstone types. Both sets exhibit distinct subgroups with varying Young's modulus (E) and Poisson's ratio (ν) values, highlighting the impact of natural heterogeneities on overall rock strength. Exposure to CO₂-acidified brine results in slightly reduced mechanical parameters compared to their intact counterparts.
- Salt crystallization stands out as a significant contributor to sandstone mechanical damage and weakening. The salt-affected specimens show a 50% reduction in Young's and shear moduli and twice an increase in Poisson's ratio compared to intact core samples. The crystallization damage was notably higher for the tighter rocks. The shear modulus (rigidity) was particularly affected. On average, the decrease in shear modulus for BBs mounts to a half and TRs to a third.
- We conceptualized two potential sets of mechanisms at pore and grain level that can be utilized to describe how salt nucleation, precipitation and growth may contribute to stress localization and mechanical damage in porous reservoir sandstones.
- The pronounced decline in rigidity and observed dilation signals the elevated risk of shear failure (when in-situ shear stress exceeds the shear strength of CO₂ storage reservoirs) in the near-wellbore regions during CO₂ injection in hypersaline aquifers. In such storage sites, there is a higher probability of extensive CO₂-induced salt growth in the evaporation front near the well-reservoir contact, where in addition to associated injectivity problems, the risk of mechanical failure exacerbated by resulting excess pressure buildup can result in integrity issues and economic consequences.

These findings may have critical implications for carbon sequestration projects in (hyper)saline aquifers. The cumulative effects of salt crystallization (coupled chemical-mechanical-hydraulic), particularly in quartz-rich sandstones, present noteworthy challenges to the integrity and economic viability of these operations. This study underscores the complexities of subsurface geochemistry-geomechanics. It emphasizes the importance of understanding, predicting, and managing these processes for the long-term integrity of geological units selected for carbon sequestration.

Acknowledgments

This work is supported by the “solid and salt precipitation kinetics during CO₂ injection into reservoir” project, funded by Norway Grants (Norwegian Financial Mechanism 2014-2021) under grant number UMO-2019/34/H/ST10/00564. H. Derluyn acknowledges the support from the European Research Council (ERC) under the European Union’s Horizon 2020 research and innovation programme (grant agreement No 850853). The authors thank Ibrahim Omar Khaled for the assistance in x-ray diffraction analysis, Salahaldin Akhavan for support in sample preparation, and Siri Simonsen for help with energy dispersive spectroscopy.

References

- Adam, L., MacFarlane, J., van Wijk*, K., Shragge, J., Higgs, K., 2015. Monitoring the effects of CO₂ injection on carbonate-cemented sandstones with elastic waves, in: SEG Technical Program Expanded Abstracts 2015, SEG Technical Program Expanded Abstracts. Society of Exploration Geophysicists, pp. 3116–3122. <https://doi.org/doi:10.1190/segam2015-5927330.1>
- Akono, A.-T., Dávila, G., Druhan, J., Shi, Z., Jessen, K., Tsotsis, T., 2020. Influence of geochemical reactions on the creep behavior of Mt. Simon sandstone. *Int. J. Greenh. Gas Control* 103. <https://doi.org/10.1016/j.ijggc.2020.103183>
- An, Q., Zhang, Q., Zhang, X., Li, X., Yu, H., Liu, Y., 2022. Influence of Mineralogy on Rock Mechanical Behaviour Considering Dynamic Alteration Damage Caused by SC-CO₂: A Comparative Study on Different Rock Types. *Rock Mech. Rock Eng.* 55, 3129–3151. <https://doi.org/10.1007/s00603-022-02807-w>
- An, S., Erfani, H., Hellevang, H., Niasar, V., 2021. Lattice-Boltzmann simulation of dissolution of carbonate rock during CO₂-saturated brine injection. *Chem. Eng. J.* 408, 127235. <https://doi.org/https://doi.org/10.1016/j.cej.2020.127235>
- Balboni, E., Espinosa-Marzal, R.M., Doehne, E., Scherer, G.W., 2011. Can drying and re-wetting of magnesium sulfate salts lead to damage of stone? *Environ. EARTH Sci.* 63, 1463–1473. <https://doi.org/10.1007/s12665-010-0774-1>
- Bjørlykke, K., 2015. Compaction of sedimentary rocks: Shales, sandstones and carbonates, in: *Petroleum Geoscience: From Sedimentary Environments to Rock Physics, Second Edition*. pp. 351–360. https://doi.org/10.1007/978-3-642-34132-8_13
- Bjørlykke, K., Jahren, J., 2015. Sandstones and sandstone reservoirs, in: *Petroleum Geoscience: From Sedimentary Environments to Rock Physics, Second Edition*. pp. 119–149. https://doi.org/10.1007/978-3-642-34132-8_4
- Brantley, S.L., Kubicki, J.D., White, A.F., 2008. Kinetics of water-rock interaction.
- Canal, J., Delgado-Martín, J., Barrientos, V., Juncosa, R., Rodríguez-Cedrún, B., Falcón-Suarez, I., 2014. Effect of supercritical CO₂ on the Corvio sandstone in a flow-thru triaxial experiment, in: *Rock Engineering and Rock Mechanics: Structures in and on Rock Masses - Proceedings of EUROCK 2014, ISRM European Regional Symposium*. pp. 1357–1362. <https://doi.org/10.1201/b16955-236>
- Chen, L., Kang, Q., Carey, B., Tao, W.-Q., 2014. Pore-scale study of diffusion–reaction processes involving dissolution and precipitation using the lattice Boltzmann method. *Int. J. Heat Mass Transf.* 75, 483–496. <https://doi.org/https://doi.org/10.1016/j.ijheatmasstransfer.2014.03.074>
- Choens, R.C., Ilgen, A.G., Espinoza, D.N., Aman, M., Wilson, J., Dewers, T.A., 2020. Impacts on mechanical strength of chemical reactions induced by hydrous supercritical CO₂ in Boise Sandstone. *Int. J. Greenh. Gas Control* 95, 102982. <https://doi.org/https://doi.org/10.1016/j.ijggc.2020.102982>
- Correns, C.W., Steinborn, W., 1939. Experiments for measuring and explaining the so-called crystallisation strength. *ZEITSCHRIFT FÜR Krist.* 101, 117–133.
- Coussy, O., 2006. Deformation and stress from in-pore drying-induced crystallization of salt. *J. Mech. Phys. Solids* 54, 1517–1547. <https://doi.org/10.1016/j.jmps.2006.03.002>
- Czernichowski-Lauriol, I., Sanjuan, B., Rochelle, C.A., Bateman, K., Pearce, J.M., Blackwell, P.A., 1996. Analysis of the geochemical aspects of the underground disposal of CO₂.
- Deng, H., Poonosamy, J., Molins, S., 2022. A reactive transport modeling perspective on the dynamics of interface-coupled dissolution-precipitation. *Appl. Geochemistry* 137, 105207. <https://doi.org/https://doi.org/10.1016/j.apgeochem.2022.105207>

- Derluyn, H., Moonen, P., Carmeliet, J., 2014. Deformation and damage due to drying-induced salt crystallization in porous limestone. *J. Mech. Phys. Solids* 63, 242–255. <https://doi.org/https://doi.org/10.1016/j.jmps.2013.09.005>
- Derluyn, H., Vontobel, P., Mannes, D., Derome, D., Lehmann, E., Carmeliet, J., 2019. Saline Water Evaporation and Crystallization-Induced Deformations in Building Stone: Insights from High-Resolution Neutron Radiography. *Transp. Porous Media* 128, 895–913. <https://doi.org/10.1007/s11242-018-1151-x>
- Desarnaud, J., Bertrand, F., Shahidzadeh-Bonn, N., 2013. Impact of the Kinetics of Salt Crystallization on Stone Damage During Rewetting/Drying and Humidity Cycling. *J. Appl. Mech.* 80. <https://doi.org/10.1115/1.4007924>
- Desarnaud, J., Bonn, D., Shahidzadeh, N., 2016. The Pressure induced by salt crystallization in confinement. *Sci. Rep.* 6, 30856. <https://doi.org/10.1038/srep30856>
- Erickson, K.P., Lempp, C., Pöllmann, H., 2015. Geochemical and geomechanical effects of scCO₂ and associated impurities on physical and petrophysical properties of Permian Sandstones (Germany): an experimental approach. *Environ. Earth Sci.* 74, 4719–4743. <https://doi.org/10.1007/s12665-015-4437-0>
- Espinosa-Marzal, R.M., Scherer, G.W., 2010. Advances in understanding damage by salt crystallization. *Acc. Chem. Res.* 43, 897–905. <https://doi.org/10.1021/ar9002224>
- Espinoza, D.N., Jung, H.J., Major, J.R., Sun, Z., Ramos, M.J., Eichhubl, P., Balhoff, M.T., Choens, R.C., Dewers, T.A., 2018. CO₂ charged brines changed rock strength and stiffness at Crystal Geyser, Utah: Implications for leaking subsurface CO₂ storage reservoirs. *Int. J. Greenh. GAS Control* 73, 16–28. <https://doi.org/10.1016/j.jggc.2018.03.017>
- Everett, D.H., 1961. The thermodynamics of frost damage to porous solids. *Trans. Faraday Soc.* 57, 1541–1551. <https://doi.org/10.1039/TF9615701541>
- Falcon-Suarez, I., North, L., Amalokwu, K., Best, A., 2016. Integrated geophysical and hydromechanical assessment for CO₂ storage: shallow low permeable reservoir sandstones. *Geophys. Prospect.* 64, 828–847. <https://doi.org/10.1111/1365-2478.12396>
- Falcon-Suarez, I.H., Livo, K., Callow, B., Marin-Moreno, H., Prasad, M., Best, A.I., 2020. Geophysical early warning of salt precipitation during geological carbon sequestration. *Sci. Rep.* 10, 16472. <https://doi.org/10.1038/s41598-020-73091-3>
- Fazeli, H., Nooraiepour, M., Hellevang, H., 2019a. Microfluidic Study of Fracture Dissolution in Carbonate-Rich Caprocks Subjected to CO₂-Charged Brine. *Ind. Eng. Chem. Res.* 59. <https://doi.org/10.1021/acs.iecr.9b06048>
- Fazeli, H., Patel, R.A., Ellis, B.R., Hellevang, H., 2019b. Three-Dimensional Pore-Scale Modeling of Fracture Evolution in Heterogeneous Carbonate Caprock Subjected to CO₂-Enriched Brine. *Environ. Sci. Technol.* 53, 4630–4639. <https://doi.org/10.1021/acs.est.8b05653>
- Flatt, R., Aly Mohamed, N., Caruso, F., Derluyn, H., Desarnaud, J., Lubelli, B., Espinosa Marzal, R.M., Pel, L., Rodriguez-Navarro, C., Scherer, G.W., Shahidzadeh, N., Steiger, M., 2017. Predicting salt damage in practice: A theoretical insight into laboratory tests. *RILEM Tech. Lett.* 2, 108–118. <https://doi.org/10.21809/rilemtechlett.2017.41>
- Flatt, R.J., 2002. Salt damage in porous materials: how high supersaturations are generated. *J. Cryst. Growth* 242, 435–454. [https://doi.org/10.1016/S0022-0248\(02\)01429-X](https://doi.org/10.1016/S0022-0248(02)01429-X)
- Flatt, R.J., Caruso, F., Sanchez, A.M.A., Scherer, G.W., 2014. Chemo-mechanics of salt damage in stone. *Nat. Commun.* 5. <https://doi.org/10.1038/ncomms5823>
- Flatt, R.J., Steiger, M., Scherer, G.W., 2007. A commented translation of the paper by CW Correns and W. Steinborn on crystallization pressure. *Environ. Geol.* 52, 221–237. <https://doi.org/10.1007/s00254-006-0509-5>
- Foroutan, M., Ghazanfari, E., 2020. CO₂-enriched brine injection's impact on mechanical properties of a sandstone specimen. *E3S Web Conf.* 205.
- Foroutan, M., Ghazanfari, E., Amirlatifi, A., 2021a. Variation of failure properties, creep response and ultrasonic velocities of sandstone upon injecting CO₂-enriched brine. *Geomech. Geophys. GEO-ENERGY GEO-RESOURCES* 7. <https://doi.org/10.1007/s40948-021-00223-y>
- Foroutan, M., Ghazanfari, E., Amirlatifi, A., Perdril, N., 2021b. Variation of pore-network, mechanical and hydrological characteristics of sandstone specimens through CO₂-enriched brine injection. *Geomech. ENERGY Environ.* 26. <https://doi.org/10.1016/j.gete.2020.100217>
- Gaus, I., 2010. Role and impact of CO₂-rock interactions during CO₂ storage in sedimentary rocks. *Int. J. Greenh. Gas Control* 4, 73–89. <https://doi.org/10.1016/j.jggc.2009.09.015>
- Godts, S., Orr, S.A., Desarnaud, J., Steiger, M., Wilhelm, K., De Clercq, H., Cnudde, V., De Kock, T., 2021. NaCl-related weathering of stone: the importance of kinetics and salt mixtures in environmental risk

- assessment. *Herit. Sci.* 9, 44. <https://doi.org/10.1186/s40494-021-00514-3>
- Guen, Yvi, Hellmann, R., Collombet, M., Gratier, J.-P.P., Renard, F., Brosse, E., Le Guen, Y, Renard, F., Hellmann, R., Brosse, E., Collombet, M., Tisserand, D., Gratier, J.-P.P., 2007. Enhanced deformation of limestone and sandstone in the presence of high P-co₂ fluids. *J. Geophys. Res. EARTH* 112. <https://doi.org/10.1029/2006JB004637>
- Guren, M.G., Putnis, C. V, Montes-Hernandez, G., King, H.E., Renard, F., 2020. Direct imaging of coupled dissolution-precipitation and growth processes on calcite exposed to chromium-rich fluids. *Chem. Geol.* 552, 119770. <https://doi.org/https://doi.org/10.1016/j.chemgeo.2020.119770>
- Hamilton, A., Koutsos, V., Hall, C., 2010. Direct measurement of salt–mineral repulsion using atomic force microscopy. *Chem. Commun.* 46, 5235–5237.
- Hangx, S., Bakker, E., Bertier, P., Nover, G., Busch, A., 2015. Chemical-mechanical coupling observed for depleted oil reservoirs subjected to long-term CO₂-exposure - A case study of the Werkendam natural CO₂ analogue field. *Earth Planet. Sci. Lett.* 428, 230–242. <https://doi.org/10.1016/j.epsl.2015.07.044>
- Hangx, S., van der Linden, A., Marcelis, F., Bauer, A., 2013. The effect of CO₂ on the mechanical properties of the Captain Sandstone: Geological storage of CO₂ at the Goldeneye field (UK). *Int. J. Greenh. Gas Control* 19, 609–619. <https://doi.org/10.1016/j.ijggc.2012.12.016>
- Hangx, S.J.T., Spiers, C.J., 2009. Reaction of plagioclase feldspars with CO₂ under hydrothermal conditions. *Chem. Geol.* 265, 88–98. <https://doi.org/https://doi.org/10.1016/j.chemgeo.2008.12.005>
- Harbert, W., Goodman, A., Spaulding, R., Haljasmaa, I., Crandall, D., Sanguinito, S., Kutchko, B., Tkach, M., Fuchs, S., Werth, C.J., Tsotsis, T., Dalton, L., Jessen, K., Shi, Z.F., Frailey, S., 2020. CO₂ induced changes in Mount Simon sandstone: Understanding links to post CO₂ injection monitoring, seismicity, and reservoir integrity. *Int. J. Greenh. GAS Control* 100. <https://doi.org/10.1016/j.ijggc.2020.103109>
- Hashemi, S.S., Kovscek, A.R., Zoback, M.D., 2022. Effect of Supercritical CO₂ on the Poroelastic Characteristics of Poorly Cemented Sandstone Reservoirs During Depletion and Injection. *SPE Annu. Tech. Conf. Exhib.* <https://doi.org/10.2118/210228-MS>
- Hu, S., Li, X., Bai, B., Shi, L., Liu, M., Wu, H., 2017. A modified true triaxial apparatus for measuring mechanical properties of sandstone coupled with CO₂-H₂O biphasic fluid. *Greenh. Gases Sci. Technol.* 7, 78–91. <https://doi.org/https://doi.org/10.1002/ghg.1637>
- Huang, Y.H., Yang, S.Q., Li, W.P., Hall, M.R., 2020. Influence of Super-Critical CO₂ on the Strength and Fracture Behavior of Brine-Saturated Sandstone Specimens. *ROCK Mech. ROCK Eng.* 53, 653–670. <https://doi.org/10.1007/s00603-019-01933-2>
- IEA, 2016. International Energy Agency: Energy Technology Perspectives.
- IEA, 2015. Carbon Capture and Storage: The Solution for Deep Emissions Reductions. *Carbon Capture Storage Solut. Deep Emiss. Reductions.*
- IPCC, 2023. Climate Change 2023: Synthesis Report. Contribution of Working Groups I, II and III to the Sixth Assessment Report of the Intergovernmental Panel on Climate Change (AR6 Synthesis Report). Geneva, Switzerland. <https://doi.org/doi:10.59327/IPCC/AR6-9789291691647>
- Kampman, N., Bickle, M., Wigley, M., Dubacq, B., 2014. Fluid flow and CO₂-fluid-mineral interactions during CO₂-storage in sedimentary basins. *Chem. Geol.* 369, 22–50. <https://doi.org/10.1016/j.chemgeo.2013.11.012>
- Kim, K., Makhnenko, R.Y., 2021. Changes in rock matrix compressibility during deep CO₂ storage. *Greenh. GASES-SCIENCE Technol.* 11, 954–973. <https://doi.org/https://doi.org/10.1002/ghg.2106>
- Kim, K., Makhnenko, R.Y., 2020. Coupling Between Poromechanical Behavior and Fluid Flow in Tight Rock. *Transp. POROUS MEDIA* 135, 487–512. <https://doi.org/10.1007/s11242-020-01484-z>
- Kim, S., Santamarina, J.C.C., 2014. CO₂ geological storage: Hydro-chemo-mechanical analyses and implications. *Greenh. Gases Sci. Technol.* 4, 528–543. <https://doi.org/10.1002/ghg.1421>
- Lamy-Chappuis, B., Angus, D., Fisher, Q.J., Yardley, B.W.D., 2016. The effect of CO₂-enriched brine injection on the mechanical properties of calcite-bearing sandstone. *Int. J. Greenh. GAS Control* 52, 84–95. <https://doi.org/10.1016/j.ijggc.2016.06.018>
- Lin, H., Fujii, T., Takisawa, R., Takahashi, T., Hashida, T., 2008. Experimental evaluation of interactions in supercritical CO₂/water/rock minerals system under geologic CO₂ sequestration conditions. *J. Mater. Sci.* 43, 2307–2315. <https://doi.org/10.1007/s10853-007-2029-4>
- Liu, F., Lu, P., Griffith, C., Hedges, S.W., Soong, Y., Hellevang, H., Zhu, C., 2012. CO₂-brine-caprock interaction: Reactivity experiments on Eau Claire shale and a review of relevant literature. *Int. J. Greenh. Gas Control* 7, 153–167. <https://doi.org/10.1016/j.ijggc.2012.01.012>
- Liu, M., Bai, B., Li, X., 2014. Experimental studies on the short term effect of CO₂ on the tensile failure of sandstone. *Energy Procedia* 63, 3357–3363. <https://doi.org/https://doi.org/10.1016/j.egypro.2014.11.364>

- Loring, J.S.S., Thompson, C.J.J., Wang, Z., Joly, A.G.G., Sklarew, D.S.S., Schaef, H.T.T., Ilton, E.S.S., Rosso, K.M.M., Felmy, A.R.R., 2011. In situ infrared spectroscopic study of forsterite carbonation in wet supercritical CO₂. *Environ. Sci. Technol.* 45, 6204–6210. <https://doi.org/10.1021/es201284e>
- Lubelli, B., Rörig-Daalgaard, I., Aguilar, A.M., Aškračić, M., Beck, K., Bläuer, C., Cnudde, V., D'Altri, A.M., Derluyn, H., Desarnaud, J., Diaz Gonçalves, T., Flatt, R., Franzoni, E., Godts, S., Gulotta, D., van Hees, R., Ioannou, I., Kamat, A., De Kock, T., Menendez, B., de Miranda, S., Nunes, C., Sassoni, E., Shahidzadeh, N., Siedel, H., Slížková, Z., Stefanidou, M., Theodoridou, M., Veiga, R., Vergès-Belmin, V., 2023. Recommendation of RILEM TC 271-ASC: New accelerated test procedure for the assessment of resistance of natural stone and fired-clay brick units against salt crystallization. *Mater. Struct.* 56, 101. <https://doi.org/10.1617/s11527-023-02158-0>
- Marbler, H., Erickson, K.P., Schmidt, M., Lempp, C., Pollmann, H., 2013. Geomechanical and geochemical effects on sandstones caused by the reaction with supercritical CO₂: an experimental approach to in situ conditions in deep geological reservoirs. *Environ. EARTH Sci.* 69, 1981–1998. <https://doi.org/10.1007/s12665-012-2033-0>
- Masoudi, M., Fazeli, H., Miri, R., Hellevang, H., 2021. Pore scale modeling and evaluation of clogging behavior of salt crystal aggregates in CO₂-rich phase during carbon storage. *Int. J. Greenh. Gas Control* 111, 103475. <https://doi.org/https://doi.org/10.1016/j.ijggc.2021.103475>
- Masoudi, M., Nooraiepour, M., Deng, H., Hellevang, H., 2024. Mineral precipitation and geometry alteration in porous structures: How to upscale variations in permeability-porosity relationship? *EarthArXiv Prepr. Arch.* <https://doi.org/10.31223/X56Q41>
- Masoudi, M., Nooraiepour, M., Hellevang, H., 2023. Salt Precipitation during Geological CO₂ Storage: Effect of Access to Continuous Brine Source. *EarthArXiv Prepr. Arch.* <https://doi.org/10.31223/X5J68G>
- Masoudi, M., Nooraiepour, M., Hellevang, H., 2022. The Effect of Preferential Nucleation Sites on the Distribution of Secondary Mineral Precipitates, in: 83rd EAGE Annual Conference & Exhibition. European Association of Geoscientists & Engineers, Madrid, Spain, pp. 1–5. <https://doi.org/https://doi.org/10.3997/2214-4609.202210445>
- Mikhaltsevitch, V., Lebedev, M., Gurevich, B., 2014. Measurements of the elastic and anelastic properties of sandstone flooded with supercritical CO₂. *Geophys. Prospect.* 62, 1266–1277. <https://doi.org/10.1111/1365-2478.12181>
- Miri, R., Hellevang, H., 2016. Salt precipitation during CO₂ storage-A review. *Int. J. Greenh. Gas Control.* <https://doi.org/10.1016/j.ijggc.2016.05.015>
- Miri, R., van Noort, R., Aagaard, P., Hellevang, H., 2015. New insights on the physics of salt precipitation during injection of CO₂ into saline aquifers. *INT J GREENH GAS CON* 43, 10–21. <https://doi.org/10.1016/j.ijggc.2015.10.004>
- Moghadam, J.N., Nooraiepour, M., Hellevang, H., Mondol, N.H., Aagaard, P., 2019. Relative permeability and residual gaseous CO₂ saturation in the Jurassic Brentskardhaugen Bed sandstones, Wilhelmøya Subgroup, western central Spitsbergen, Svalbard. *Nor. J. Geol.* 99, 1–12. <https://doi.org/10.17850/njg005>
- Nadelman, E.I., Kurtis, K.E., 2019. Durability of Portland-limestone cement-based materials to physical salt attack. *Cem. Concr. Res.* 125. <https://doi.org/10.1016/j.cemconres.2019.105859>
- Nooraiepour, M., 2022. Clay Mineral Type and Content Control Properties of Fine-Grained CO₂ Caprocks—Laboratory Insights from Strongly Swelling and Non-Swelling Clay—Quartz Mixtures. *Energies.* <https://doi.org/10.3390/en15145149>
- Nooraiepour, M., 2018. Rock properties and sealing efficiency in fine-grained siliciclastic caprocks — Implications for CCS and petroleum industry. *Fac. Math Nat. Sci, Dep Geosci. University of Oslo, Oslo, Norway.*
- Nooraiepour, M., Bohloli, B., Park, J., Sauvin, G., Skurtveit, E., Mondol, N.H.H., 2018. Effect of brine-CO₂ fracture flow on velocity and electrical resistivity of naturally fractured tight sandstones. *Geophysics* 83, WA37–WA48. <https://doi.org/10.1190/GEO2017-0077.1>
- Nooraiepour, M., Fazeli, H., Miri, R., Hellevang, H., 2019. Salt Precipitation during Injection of CO₂ into Saline Aquifers: Lab-on-Chip Experiments on Glass and Geomaterial Microfluidic Specimens. *SSRN Electron. J. Proc. 14th Greenh. Gas Control Technol. Conf.* <https://doi.org/10.2139/ssrn.3365553>
- Nooraiepour, Mohammad, Fazeli, H., Miri, R., Hellevang, H., 2018. Effect of CO₂ Phase States and Flow Rate on Salt Precipitation in Shale Caprocks - A Microfluidic Study. *Environ. Sci. Technol.* 52, 6050–6060. <https://doi.org/10.1021/acs.est.8b00251>
- Nooraiepour, M., Haile, B.G., Hellevang, H., 2017. Compaction and mechanical strength of Middle Miocene mudstones in the Norwegian North Sea – The major seal for the Skade CO₂ storage reservoir. *Int. J. Greenh. Gas Control* 67. <https://doi.org/10.1016/j.ijggc.2017.10.016>

- Nooraiepour, M., Masoudi, M., Hellevang, H., 2021a. Probabilistic nucleation governs time, amount, and location of mineral precipitation and geometry evolution in the porous medium. *Sci. Rep.* 11. <https://doi.org/10.1038/s41598-021-95237-7>
- Nooraiepour, M., Masoudi, M., Shokri, N., Hellevang, H., 2021b. Probabilistic Nucleation and Crystal Growth in Porous Medium: New Insights from Calcium Carbonate Precipitation on Primary and Secondary Substrates. *ACS Omega* 6, 28072–28083. <https://doi.org/10.1021/acsomega.1c04147>
- Nooraiepour, M., Masoudi, M., Shokri, N., Hellevang, H., 2022. Precipitation-induced Geometry Evolution in Porous Media: Numerical and Experimental Insights based on New Model on Probabilistic Nucleation and Mineral Growth. *SSRN Electron. J. Proc. 16th Greenh. Gas Control Technol. Conf.* <https://doi.org/10.2139/ssrn.4272555>
- Nooraiepour, Mohammad, Mondol, N.H., Hellevang, H., 2019. Permeability and physical properties of semi-compacted fine-grained sediments – A laboratory study to constrain mudstone compaction trends. *Mar. Pet. Geol.* <https://doi.org/10.1016/j.marpetgeo.2019.01.019>
- Nooraiepour, Mohammad, Mondol, N.H., Hellevang, H., Bjørlykke, K., 2017. Experimental mechanical compaction of reconstituted shale and mudstone aggregates: Investigation of petrophysical and acoustic properties of SW Barents Sea cap rock sequences. *Mar. Pet. Geol.* 80, 265–292. <https://doi.org/10.1016/j.marpetgeo.2016.12.003>
- Norouzi, A.M., Niasar, V., Gluyas, J.G., Babaei, M., 2022. Analytical Solution for Predicting Salt Precipitation During CO₂ Injection Into Saline Aquifers in Presence of Capillary Pressure. *Water Resour. Res.* 58, e2022WR032612. <https://doi.org/https://doi.org/10.1029/2022WR032612>
- Nover, G., Von Der Gonna, J., Heikamp, S., Koster, J., 2013. Changes of petrophysical properties of sandstones due to interaction with supercritical carbon dioxide - a laboratory study. *Eur. J. Mineral.* 25, 317–329. <https://doi.org/10.1127/0935-1221/2013/0025-2295>
- Orlander, T., Andreassen, K.A., Fabricius, I.L., 2021. Effect of Temperature on Stiffness of Sandstones from the Deep North Sea Basin. *Rock Mech. Rock Eng.* 54, 255–288. <https://doi.org/10.1007/s00603-020-02251-8>
- Ott, H., Snippe, J., de Kloe, K., 2021. Salt precipitation due to supercritical gas injection: II. Capillary transport in multi porosity rocks. *Int. J. Greenh. Gas Control* 105, 103233. <https://doi.org/https://doi.org/10.1016/j.ijggc.2020.103233>
- Palandri, J.L., Kharaka, Y.K., 2004. A compilation of rate parameters of water-mineral interaction kinetics for application to geochemical modeling.
- Parvin, S., Masoudi, M., Sundal, A., Miri, R., 2020. Continuum scale modelling of salt precipitation in the context of CO₂ storage in saline aquifers with MRST compositional. *Int. J. Greenh. Gas Control* 99, 103075. <https://doi.org/https://doi.org/10.1016/j.ijggc.2020.103075>
- Pearce, J.K., Dawson, G.K.W., Law, A.C.K., Biddle, D., Golding, S.D., 2016. Reactivity of micas and cap-rock in wet supercritical CO₂ with SO₂ and O₂ at CO₂ storage conditions. *Appl. Geochemistry* 72, 59–76. <https://doi.org/https://doi.org/10.1016/j.apgeochem.2016.06.010>
- Perera, M.S.A., Rathnaweera, T.D., Ranjith, P.G., Wanniarachchi, W.A.M., Nasvi, M.C.A., Abdulagatov, I.M., Haque, A., 2016. Laboratory measurement of deformation-induced hydro-mechanical properties of reservoir rock in deep saline aquifers: An experimental study of Hawkesbury formation. *Mar. Pet. Geol.* 77, 640–652. <https://doi.org/10.1016/j.marpetgeo.2016.07.012>
- Pham, V.T.H., Lu, P., Aagaard, P., Zhu, C., Hellevang, H., 2011. On the potential of CO₂–water–rock interactions for CO₂ storage using a modified kinetic model. *Int. J. Greenh. Gas Control* 5, 1002–1015. <https://doi.org/https://doi.org/10.1016/j.ijggc.2010.12.002>
- Pitzer, K.S., 1991. *Activity Coefficients in Electrolyte Solutions*, 2nd editio. ed. CRC Press. <https://doi.org/https://doi.org/10.1201/9781351069472>
- Prasianakis, N.I., Curti, E., Kosakowski, G., Poonoosamy, J., Churakov, S. V., 2017. Deciphering pore-level precipitation mechanisms. *Sci. Rep.* 7, 13765. <https://doi.org/10.1038/s41598-017-14142-0>
- Qazi, M.J., Salim, H., Doorman, C.A.W., Jambon-Puillet, E., Shahidzadeh, N., 2019. Salt creeping as a self-amplifying crystallization process. *Sci. Adv.* 5. <https://doi.org/10.1126/sciadv.aax1853>
- Rahman, M.J., Fawad, M., Chan Choi, J., Mondol, N.H., 2022. Effect of overburden spatial variability on field-scale geomechanical modeling of potential CO₂ storage site Smeaheia, offshore Norway. *J. Nat. Gas Sci. Eng.* 99, 104453. <https://doi.org/https://doi.org/10.1016/j.jngse.2022.104453>
- Ranjith, P.G., Viete, D.R., Chen, B.J., Perera, M.S.A., 2012. Transformation plasticity and the effect of temperature on the mechanical behaviour of Hawkesbury sandstone at atmospheric pressure. *Eng. Geol.* 151, 120–127. <https://doi.org/https://doi.org/10.1016/j.enggeo.2012.09.007>
- Rathnaweera, T.D., Ranjith, P.G., Perera, M.S.A., Ranathunga, A.S., Wanniarachchi, W.A.M., Yang, S.Q., Lashin, A., Al Arifi, N., 2017. An experimental investigation of coupled chemico-mineralogical and mechanical

- changes in variably-cemented sandstones upon CO₂ injection in deep saline aquifer environments. *ENERGY* 133, 404–414. <https://doi.org/10.1016/j.energy.2017.05.154>
- Rathnaweera, T.D.D., Ranjith, P.G.G., Perera, M.S.A.S.A., Haque, A., Lashin, A., Al Arifi, N., Chandrasekharan, D., Yang, S.Q.Q., Xu, T., Wang, S.H.H., Yasar, E., Wang, S.H.H., Yasar, E., 2015. CO₂-induced mechanical behaviour of Hawkesbury sandstone in the Gosford basin: An experimental study. *Mater. Sci. Eng. A* 641, 123–137. <https://doi.org/10.1016/j.msea.2015.05.029>
- Raza, A., Gholami, R., Sarmadivaleh, M., Tarom, N., Rezaee, R., Bing, C.H., Nagarajan, R., Hamid, M.A., Elochukwu, H., 2016. Integrity analysis of CO₂ storage sites concerning geochemical-geomechanical interactions in saline aquifers. *J. Nat. Gas Sci. Eng.* 36, 224–240. <https://doi.org/10.1016/j.jngse.2016.10.016>
- Rimmele, G., Barlet-Gouédard, V., Renard, F., Rimmelé, G., Barlet-Gouédard, V., Renard, F., 2010. Evolution of the Petrophysical and Mineralogical Properties of Two Reservoir Rocks Under Thermodynamic Conditions Relevant for CO₂ Geological Storage at 3 km Depth. *OIL GAS Sci. Technol. D IFP ENERGIES Nouv.* 65, 565–580. <https://doi.org/10.2516/ogst/2009071>
- Rinehart, A.J., Dewers, T.A., Broome, S.T., Eichhubl, P., 2016. Effects of CO₂ on mechanical variability and constitutive behavior of the Lower Tuscaloosa Formation, Cranfield Injection Site, USA. *Int. J. Greenh. GAS Control* 53, 305–318. <https://doi.org/10.1016/j.jggc.2016.08.013>
- Ringrose, P.S., Furre, A.-K., Gilfillan, S.M. V, Krevor, S., Landroslash, M., Leslie, R., Meckel, T., Nazarian, B., Zahid, A., 2021. Storage of Carbon Dioxide in Saline Aquifers: Physicochemical Processes, Key Constraints, and Scale-Up Potential. *Annu. Rev. Chem. Biomol. Eng.* 12, 471–494. <https://doi.org/10.1146/annurev-chembioeng-093020-091447>
- Ringrose, P.S.S., Meckel, T.A.A., 2019. Maturing global CO₂ storage resources on offshore continental margins to achieve 2DS emissions reductions. *Sci. Rep.* 9. <https://doi.org/10.1038/s41598-019-54363-z>
- Rohmer, J., Pluymakers, A., Renard, F., 2016. Mechano-chemical interactions in sedimentary rocks in the context of CO₂ storage: Weak acid, weak effects? *Earth-Science Rev.* 157, 86–110. <https://doi.org/10.1016/j.earscirev.2016.03.009>
- Rosenbauer, R.J., Koksalan, T., Palandri, J.L., 2005. Experimental investigation of CO₂-brine-rock interactions at elevated temperature and pressure: Implications for CO₂ sequestration in deep-saline aquifers. *Fuel Process. Technol.* 86, 1581–1597. <https://doi.org/10.1016/j.fuproc.2005.01.011>
- Rutqvist, J., Birkholzer, J.T., Tsang, C.-F., 2008. Coupled reservoir–geomechanical analysis of the potential for tensile and shear failure associated with CO₂ injection in multilayered reservoir–caprock systems. *Int. J. Rock Mech. Min. Sci.* 45, 132–143. <https://doi.org/10.1016/j.ijrmms.2007.04.006>
- Samuelson, J., Spiers, C.J., 2012. Fault friction and slip stability not affected by CO₂ storage: Evidence from short-term laboratory experiments on North Sea reservoir sandstones and caprocks. *Int. J. Greenh. GAS Control* 11, S78–S90. <https://doi.org/10.1016/j.jggc.2012.09.018>
- Scherer, G.W.W., 2004. Stress from crystallization of salt. *Cem. Concr. Res.* 34, 1613–1624. <https://doi.org/10.1016/j.cemconres.2003.12.034>
- Scherer, G.W.W., Flatt, R., Wheeler, G., 2001. Materials science research for the conservation of sculpture and monuments. *MRS Bull.* 26, 44–50. <https://doi.org/10.1557/mrs2001.18>
- Schimmel, M.T.W., Hangx, S.J.T., Spiers, C.J., 2022. Effect of pore fluid chemistry on uniaxial compaction creep of Bentheim sandstone and implications for reservoir injection operations. *Geomech. ENERGY Environ.* 29. <https://doi.org/10.1016/j.gete.2021.100272>
- Shahidzadeh-Bonn, N., Desarnaud, J., Bertrand, F., Chateau, X., Bonn, D., 2010. Damage in porous media due to salt crystallization. *Phys. Rev. E* 81, 66110. <https://doi.org/10.1103/PhysRevE.81.066110>
- Shao, J., You, L., Kang, Y., Chen, M., 2022. Experimental investigation of effect of salt crystallization on the mechanical strength of shale. *J. Pet. Sci. Eng.* 213, 110366. <https://doi.org/10.1016/j.petrol.2022.110366>
- Sharifi, J., Nooraiepour, M., Amiri, M., Mondol, N.H., 2023. Developing a relationship between static Young's modulus and seismic parameters. *J. Pet. Explor. Prod. Technol.* 13, 203–218. <https://doi.org/10.1007/s13202-022-01546-6>
- Sharifi, J., Nooraiepour, M., Mondol, N.H., 2021. Application of the Analysis of Variance for Converting Dynamic to Static Young's Modulus, in: 82nd EAGE Conference and Exhibition 2021. pp. 2587–2591.
- Shi, Z., Sun, L., Haljasmaa, I., Harbert, W., Sanguinito, S., Tkach, M., Goodman, A., Tsotsis, T.T., Jessen, K., 2019. Impact of Brine/CO₂ exposure on the transport and mechanical properties of the Mt Simon sandstone. *J. Pet. Sci. Eng.* 177, 295–305. <https://doi.org/10.1016/j.petrol.2019.01.112>
- Shokri-Kuehni, S.M.S., Bergstad, M., Sahimi, M., Webb, C., Shokri, N., 2018. Iodine k-edge dual energy imaging reveals the influence of particle size distribution on solute transport in drying porous media. *Sci. Rep.* 8,

10731. <https://doi.org/10.1038/s41598-018-29115-0>
- Skurtveit, E., Torabi, A., Sundal, A., Braathen, A., 2021. The role of mechanical stratigraphy on CO₂ migration along faults – examples from Entrada Sandstone, Humberg Flats, Utah, USA. *Int. J. Greenh. Gas Control* 109, 103376. <https://doi.org/10.1016/j.ijggc.2021.103376>
- Song, J., Zhang, D., 2013. Comprehensive review of caprock-sealing mechanisms for geologic carbon sequestration. *Env. Sci Technol* 47, 9–22. <https://doi.org/10.1021/es301610p>
- Steiger, M., 2005a. Crystal growth in porous materials - I: The crystallization pressure of large crystals. *J. Cryst. Growth* 282, 455–469. <https://doi.org/10.1016/j.jcrysgro.2005.05.007>
- Steiger, M., 2005b. Crystal growth in porous materials - II: Influence of crystal size on the crystallization pressure. *J. Cryst. Growth* 282, 470–481. <https://doi.org/10.1016/j.jcrysgro.2005.05.008>
- Sun, L., Jessen, K., Tsotsis, T.T., 2021. Impact of exposure to brine/CO₂ on the mechanical and transport properties of the Mt. Simon Sandstone. *Greenh. Gases Sci. Technol.* 11, 1043–1055. <https://doi.org/10.1002/ghg.2115>
- Sun, Q., Lü, C., Cao, L., Li, W., Geng, J., Zhang, W., 2016. Thermal properties of sandstone after treatment at high temperature. *Int. J. Rock Mech. Min. Sci.* 85, 60–66. <https://doi.org/10.1016/j.ijrmms.2016.03.006>
- Sun, Z., Song, X., Feng, G., Huo, Y., Kong, S., Zhu, D., 2019. Experimental study on the fracture behavior of sandstone after ScCO₂–water–rock interaction. *J. Nat. Gas Sci. Eng.* 68, 102904. <https://doi.org/10.1016/j.jngse.2019.102904>
- Sun, Z., Song, X., Feng, G., Huo, Y., Wang, Z.-L., Kong, S., 2020. Influence of supercritical, liquid, and gaseous CO₂ on fracture behavior in sandstone. *Energy Sci. Eng.* 8, 3788–3804. <https://doi.org/10.1002/ese3.736>
- Tariq, Z., Abdurraheem, A., Elkatatny, S., Mahmoud, M., Muqtadir, A., Murtaza, M., 2018. Geomechanical studies on CO₂ sequestered rocks in an aqueous saline environment, in: SPE Kingdom of Saudi Arabia Annual Technical Symposium and Exhibition. SPE, p. SPE-192242.
- Tarokh, A., Makhnenko, R.Y., Kim, K., Zhu, X., Popovics, J.S., Segvic, B., Sweet, D.E., 2020. Influence of CO₂ injection on the poromechanical response of Berea sandstone. *Int. J. Greenh. Gas Control* 95, 102959. <https://doi.org/10.1016/j.ijggc.2020.102959>
- Tutolo, B.M., Luhmann, A.J., Kong, X.-Z., Saar, M.O., Seyfried, W.E., 2015. CO₂ sequestration in feldspar-rich sandstone: Coupled evolution of fluid chemistry, mineral reaction rates, and hydrogeochemical properties. *Geochim. Cosmochim. Acta* 160, 132–154. <https://doi.org/10.1016/j.gca.2015.04.002>
- Vafaie, A., Cama, J., Soler, J.M., Kivi, I.R., Vilarrasa, V., 2023. Chemo-hydro-mechanical effects of CO₂ injection on reservoir and seal rocks: A review on laboratory experiments. *Renew. Sustain. Energy Rev.* 178, 113270. <https://doi.org/10.1016/j.rser.2023.113270>
- Vanorio, T., Nur, A., Ebert, Y., 2011. Rock physics analysis and time-lapse rock imaging of geochemical effects due to the injection of CO₂ into reservoir rocks. *Geophysics* 76, O23–O33. <https://doi.org/10.1190/geo2010-0390.1>
- Vilarrasa, V., Olivella, S., Carrera, J., Rutqvist, J., 2014. Long term impacts of cold CO₂ injection on the caprock integrity. *Int. J. Greenh. Gas Control* 24, 1–13. <https://doi.org/10.1016/j.ijggc.2014.02.016>
- Wang, X., Wang, L., Zhao, B., Wu, Y., Yang, J., Sun, J., 2022. Experimental Study on Mechanical Properties of Gas Storage Sandstone and Its Damage Under Temperature and Pressure. *Front. Earth Sci.*
- Watts, N.L., 1987. Theoretical aspects of cap-rock and fault seals for single- and two-phase hydrocarbon columns. *Mar. Pet. Geol.* 4, 274–307. [https://doi.org/10.1016/0264-8172\(87\)90008-0](https://doi.org/10.1016/0264-8172(87)90008-0)
- Wu, Z., Luhmann, A., Rinehart, A., Mozley, P., Dewers, T., Heath, J., Majumdar, B., 2018. Controls of cement texture and composition on sandstone mechanical property changes from reaction with CO₂-rich brine, in: AAPG ACE 2018.
- Yu, S., Oguchi, C.T., 2010. Role of pore size distribution in salt uptake, damage, and predicting salt susceptibility of eight types of Japanese building stones. *Eng. Geol.* 115, 226–236. <https://doi.org/10.1016/j.enggeo.2009.05.007>
- Zhang, D., Kang, Y., Selvadurai, A.P.S., You, L., 2020. Experimental Investigation of the Effect of Salt Precipitation on the Physical and Mechanical Properties of a Tight Sandstone. *Rock Mech. Rock Eng.* 53, 4367–4380. <https://doi.org/10.1007/s00603-019-02032-y>
- Zhang, M., Bachu, S., 2011. Review of integrity of existing wells in relation to CO₂ geological storage: What do we know? *Int. J. Greenh. Gas Control* 5, 826–840. <https://doi.org/10.1016/j.ijggc.2010.11.006>
- Zhang, P., Tian, S., Ren, S., Wu, F., Chen, J., Ma, L., 2023. Effects of high temperature and acidic solutions on

- the pore characteristics and mechanical properties of sandstone. *Environ. Sci. Pollut. Res.* 30, 21888–21899. <https://doi.org/10.1007/s11356-022-23735-w>
- Zhang, Y., Sarmadivaleh, M., Lebedev, M., Barifcani, A., Rezaee, R., Testamantia, N., Iglauer, S., 2016. Geo-Mechanical Weakening of Limestone Due to Supercritical CO₂ Injection. <https://doi.org/10.4043/26470-ms>
- Zhao, D.F., Liao, X.W., Yin, D.D., 2015. An experimental study for the effect of CO₂-brine-rock interaction on reservoir physical properties. *J. Energy Inst.* 88, 27–35. <https://doi.org/https://doi.org/10.1016/j.joei.2014.05.001>
- Zheng, H., Feng, X.-T., Pan, P.-Z., 2015. Experimental investigation of sandstone properties under CO₂-NaCl solution-rock interactions. *Int. J. Greenh. Gas Control* 37, 451–470. <https://doi.org/https://doi.org/10.1016/j.ijggc.2015.04.005>
- Zhou, H., Hu, D.W., Zhang, F., Shao, J.F., Feng, X.T., 2016. Laboratory Investigations of the Hydro-Mechanical-Chemical Coupling Behaviour of Sandstone in CO₂ Storage in Aquifers. *ROCK Mech. ROCK Eng.* 49, 417–426. <https://doi.org/10.1007/s00603-015-0752-8>
- Zhu, H., Xu, T., Tian, H., Feng, G., Yang, Z., Zhou, B., 2019. Understanding of Long-Term CO₂-Brine-Rock Geochemical Reactions Using Numerical Modeling and Natural Analogue Study. *Geofluids* 2019, 1426061. <https://doi.org/10.1155/2019/1426061>

1 Appendix

2

3 **Table 1.** Chemo-mechanical interactions of CO₂ (dry, wet and water/bine-acidified) with sandstone rock type in natural environments and laboratory settings, including natural seepage (NS), batch (B) and flow-through (F) experiments.

4

Literature	Sample	Test Type & Duration	Test Conditions (MPa & °C)	Carbonate Content	Carbonate Type	ϕ_i	ϕ_f	k_i	k_f	E_i	E_f	K_i	K_f	ν_i	ν_f	UCS _i	UCS _f	Remarks
(Espinoza et al., 2018)	Summerville (USA)	NS	--	23-43	sparry calcite and micritic calcite cement	4.8 ± 1.6	10.2 ± 0.4			32,80	7,60			0,22	0,15	159	20,4	CO ₂ -charged brine induces time-dependent reductions in stiffness, strength, and brittleness in sedimentary rocks. Localized leakage alters deformational behavior and mechanical properties substantially.
(Espinoza et al., 2018)	Entrada (USA)	NS	--	14	5.5: sparry calcite	8.3±0.4	11.6±0.3			20	14			0,32	0,3	66,1	57	same as above
(Hangx et al., 2015)	Röt Fringe (Netherlands)	NS	--	2-29(46)	0-0.4: calcite, 0.5-9: siderite, and mostly dolomite	7	7	0,276	0,276	19	21	20,1	22,7			117		Pre-CO ₂ injection rock parameters predict reservoir long-term mechanical behavior, unless CO ₂ reactions dissolve framework-supporting elements. Concentrated early diagenetic cements, if reactive, may weaken porous sandstones, impacting storage site integrity. Screening for such cements is advised.
(Skurtveit et al., 2021)	Entrada (USA)	NS	--	?		7-15	15-25	3-200	20-3000	3-14						34-65	19.7	Bleaching and Fe-oxide removal show unclear strength reduction indications.
(Adam et al., 2015)	Taranki (New Zealand)	B (48 h)	2.76 & ?	0.3-32		4.5-11												Matrix weakening impact rivals CO ₂ -water substitution. Pronounced velocity changes occur in larger-grained, high-porosity sandstones, primarily due to dissolution.
(Rathnaweera et al., 2017)	Hawkesbury (Australia)	B (12 months)	4-10 & 35	7 & 30	calcite	29 & 28		103 & 94								54-57 & 48-52		CO ₂ injection induces strength gain in silica-cemented sandstone aquifers via quartz precipitation. Conversely, carbonate-cemented sandstone formations experience mechanical weakening due to calcite dissolution at grain-to-grain contacts during CO ₂ interaction.
(Marbler et al., 2013)	- Birkigt Triassic sandstone(silicate) - Uder Triassic sandstone(carbonate) - Bebertal Permian sandstone(silicate-carbonate) (Germany)	B (12-35 days)	10 & 100	0 25 4-5	calcite	23-28 27 12-23				10.8-13.1 11.9-15.5 16.7-22.4								Autoclave treatment induces geochemical alterations, particularly in carbonate and sheet silicate cements, impacting the granular structure of sandstones. Exposure to pure scCO ₂ results in reduced strength, modified elastic deformation, and altered effective porosity compared to untreated sandstones.
(Zhao et al., 2015)	Xinghe (China)	B/F (5 days)	15-25 & 50/100	20,7	8,6: calcite 12,1: dolomite	8,4	8,2	756	363									CO ₂ -brine-rock interaction worsens rock permeability and raises displacement pressure. Reduced permeability is linked to altered pore structure, attributed to corrosion, secondary mineral formation, and precipitation. The distribution shift towards medium-sized throats is a key outcome.
(An et al., 2022)	Laizhou (China)	B/F (1-7 days)	15 & 200	20,1	calcite	13,1				7,1	4-5.5					63,7	27-48	SC-CO ₂ alters rock strength, decreasing quartz, increasing feldspar. Calcite dissolution dominates in 7 days. Dynamic alteration weakens soluble mineral dissolution, promoting insoluble mineral spallation. Insoluble minerals control altered rock strength; ISR index mirrors changes; highest reaction order influences damage rate.
(Hu et al., 2017)	Zigong (China)	B (6 h)	10 & 50	10.6	calcite	8,8		0,042										Pore-fluid and mineral interactions involve complex ion exchange, adsorption, and chemical dissolution. In CO ₂ -bearing sandstone, brittle failure prevails, while H ₂ O-bearing sandstone exhibits plasticity.
(Choens et al., 2020)	Boise (USA)	B (1-7 days)	13,8 & 70	9	calcite	29				~8	~8			0,1	0,12			Exposure to hydrous supercritical CO ₂ weakens without a direct correlation between dissolution and weakening. Quartz-cemented sandstones in storage

																			reservoirs may not see significant changes. Sandstones with vulnerable cementing phases could be adversely affected by hydrous supercritical CO ₂ .
(Samuelson and Spiers, 2012)	Hardeggen Bunter (Netherlands)	F	15 & 113-117	8	dolomite														Supercritical CO ₂ shows no discernible impact on the coefficient of friction. Short-term effects do not enhance fault zone reactivation, as there's no apparent reduction in frictional strength during CO ₂ injection-induced stress changes.
(Rathnaweera et al., 2015)	Hawkesbury (Australia)	B (4 months)	8 & 32	7	5: calcite 2: siderite	37				10.3	4.2			0.26	0.32				Supercritical CO ₂ injection induces reservoir rock weakening, attributed to CO ₂ -water-rock mineral interaction, producing carbonic acid and causing quartz corrosion. Additionally, CO ₂ -rock mineral interaction contributes to mineral dissolution in the rock mass.
(Foroutan and Ghazanfari, 2020)	Pecos (USA)	F (72 h)	7.5-21.5 & ?	7	calcite					23-27	21-22	6,5	5	0,17-0.19	0,24-0.27				Enriched brine injection induces significant deterioration in elastic properties, heightened plastic deformation, and notable hysteresis behavior.
(Foroutan et al., 2021a, 2021b)	Pecos(USA)	F (63 h)	7.5-21.5 & 25	7	calcite	4	7			27,5	21,7	26,2	16,6						Notable degradation in elastic properties, particularly Young's modulus, is evident, attributable to weakened mineral grain bonding.
(Perera et al., 2016)	Quartz-cemented Hawkesbury (Australia)	B (2 years)	10 & 35	6	5: calcite 1: siderite	27	29	90	98,1	9,6	8,3			0,26	0,36	26	20		Excessive overburden pressure in saline aquifers during CO ₂ sequestration may weaken the reservoir rock mass, leading to reservoir subsidence.
(Hashemi et al., 2022)	West Delta (USA)	B (24 h)	10-40 & 42	4,5	?	23,1		3,81											Elastic modulus increased after almost 20 days of scCO ₂ exposure during injection, possibly due to scCO ₂ absorption into clay minerals and specimen dehydration.
(Zhou et al., 2016)	Red sandstone (China)	F (250 days)	3-8 & 40	4	calcite	21		3,1	30,1	7,9	4,9	6,9		0,21	0,21				Fluid-rock reaction induced notable creep deformation, decreased permeability in CO ₂ -brine creep tests, and led to elastic modulus degradation in indentation tests.
(Guen et al., 2007)	Triassic arkosic sandstone (France)	F (70 days)	8,3 & 40	3 (?)	?		15,8	17,5	461										Percolation of CO ₂ -rich fluids impacts aquifer compaction behavior, influencing long-term CO ₂ storage and sequestration capacity.
(Mikhailsevitch et al., 2014)	Donnybrook (Australia)	F (48 h)	10 & 42	2	siderite	11.5		0,276				16,3	12,9						P-velocities decrease post-scCO ₂ injection, aligning closely with the difference between water-saturated and dry samples. Extensional attenuation remains practically unchanged in water-saturated sandstone before and after scCO ₂ injection.
(Raza et al., 2016)	Berea (USA)	F (24 h)	14 & 35	2	ankerite	19		420		25,3				0,25	0,25	53			Shear velocity and modulus reductions are attributed to clay corrosion and calcite dissolution in the matrix.
(Shi et al., 2019)	Mt. Simon (USA)	B/F (7-14 days)	14-17 & 45-50	2	ankerite and dolomite	21	23	9,67	34,3	14	13,2	5,2	4,9						Mt. Simon Sandstone undergoes significant changes in both transport and mechanical properties when exposed to CO ₂ /brine within a short 1–2 week period.
(Harbert et al., 2020)	Mt. Simon (USA)	B (30 days)	13 & 53	2	ankerite and dolomite	17	18	2,6	8	17,1	12	7,2	5,3	0,11	0,13				CO ₂ /brine-induced geochemical alterations and mineral framework interactions weaken mineral strength at grain boundaries, fostering fracture propagation or generating new fractures along bedding planes.
(Harbert et al., 2020)	Mt. Simon (USA)	B (30 days)	13 & 53	2	ankerite and dolomite	24	21	380	405	16,2	19,4	7,5	10,1	0,13	0,17				Slight brittleness reduction and -9% porosity change post-CO ₂ /brine exposure. Reduced pore space may contribute to increased local strain.
(Tarokh et al., 2020)	Berea (USA)	F (22 days)	6.9 & 22	1	Fe-dolomite	25,1		148	296										CO ₂ treatment significantly alters Berea sandstone's poroviscoelastic behavior. Water-saturated specimens exhibit over twice the time-dependent deformation rate under constant load compared to pristine and damaged states.
(Sun et al., 2021)	Mt. Simon (USA)	B (21 days)		0,8	calcite	16	22,2	9	30,3	15	12,5								Core incubation in CO ₂ /brine induces mechanical changes, with estimated Young's modulus suggesting potential structure weakening post-exposure.
(Hangx et al., 2013)	Captain D (England)	F (1-2 days)	14 & 20-60	0,3	calcite	29				21,7	16,3	13,6	8,8	0,24	0,18	80,2	74,1		Calcite dissolution, but grain-to-grain contacts are sufficiently quartz-cemented, preventing significant

																		weakening. No shear failure is expected during CO2 injection, minimizing fines production. However, in shallower, less quartz-cemented sandstones, calcite dissolution may pose a risk. Investigating the short-term effects of CO2 injection on mechanical properties is crucial for such formations.
(Canal et al., 2014)	Corvio (Spain)	F (24 days)	8 & 40	0,05		14,5				11,4				0,38		41,3		Interlinked hydro-mechanical processes dominate, with a minor contribution from reactive phenomena.
(Nooraiepour et al., 2018)	De Geerdalen (Norway)	F (+100 h)	9 & 19-21	minor		<2.5		<0.01		29,37						139,23		CO2 injection-induced drying in swelled sandstone reinstated initial fracture permeability.
(Rimmele et al., 2010)	Adamswiller (France)	F (30 days)	28 & 90	0		23	26	10,8	108			6	6	0,25	0,25	25	25	Mechanical properties remain unchanged, while porosity increases after CO2 exposure.
(Vanorio et al., 2011)	Fontainebleau (France)	F (?)	15 & 25	0		15	12	1720	1380									CO2 injection induces chemo-mechanical alterations in reservoir rocks, impacting baseline transport and elastic properties. Consideration of these changes is essential for accurate interpretation of 4D seismic anomalies in rock-physics models.
(Nover et al., 2013)	Bernburg, Volperiehauser, Neidenbach (Germany)	B (10-180 days)	10-20 & 100/200	0		15	16	1,1	3,3					0,26	0,36			Low-frequency electrical conductivity experiments show a notable increase, attributed to dissolution at narrow pore throats enhancing pore system interconnection. A phase angle shift suggests alterations in the geometry of the pore-surface area.
(Falcon-Suarez et al., 2016)	Synthetic	F (172 h)	8.2 & 35	0		26		1	1,32									Velocity changes and energy loss observed with CO2 saturation are linked to heterogeneous fluid distribution within the sandstone pores, not internal solid skeleton discontinuities.
(Rinehart et al., 2016)	Tuscaloosa (USA)	F (<1 day)	13 & 100	0		19	19									65	35	Creep strain rates accelerate in facies with more chlorite cements in brine-CO2 solutions. Weakened grain-to-grain contacts lead to earlier-than-expected initial yield, associated with chemically-controlled failure envelope lowering under acidic conditions induced by CO2 in pore solutions.
(Tariq et al., 2018)	Berea (USA)	B (10-120 days)	8.27 & 120	0		17	17	199	199	32,08	20,16			0,1	0,1			CO2 significantly affected petrophysical and mechanical parameters of the studied rocks.
(Huang et al., 2020)	Zunyi (China)	F (24 h)	10 & 32	0		18		900								40	30	Brine-scCO2 co-saturation lowered UCS, Brazilian tensile strength, and fracture toughness in sandstone compared to brine-saturated specimens. scCO2 had no significant impact on fracture behavior. Strength reduction was attributed to altered pore structure from clay-cementation (kaolinite) dissolution in acidic solution.
(Kim and Makhnenko, 2021, 2020)	Berea (USA)	B&F (21 days)	7 & 22	0		22	22	100				30	30					CO2-water mixture has negligible impact on silica-rich rock and quartz compressibility. However, for calcite-rich rocks and calcite, bulk moduli decrease by 15–21%.
(Sun et al., 2020, 2019)	Datong (China)	B (10-30 days)	8 & 40	0												64.7		ScCO2 + water immersion time reduces sandstone fracture toughness. Prolonged saturation induces pore and crack formation, progressively deteriorating the structure and weakening fracture resistance.
(Liu et al., 2014)	Zigong (China)	B	1-6 & 25	0				86										Tensile fracturing of sandstone remained largely unaffected by gaseous CO2, with or without the combined effect of water.
(Schimmel et al., 2022)	Bentheim (Germany)	B	10 & 80	0		21.8–23.3												Injection of acidic fluids is likely to impede reservoir compaction.
(Akono et al., 2020)	Mt. Simon (USA)	F/B (5/7 days)	8,6/17,2 & 50-53	0	0	23-40												CO2-induced geochemical reactions lead to microstructural changes, causing a significant decrease in the macroscopic logarithmic creep modulus.
(Zhang et al., 2023)	Sichuan (China)	B (7 days)	0.1 & 25	0		6	7.5			9.5	8					77	65	Acidic solution effectively reduced compressive strength and elastic modulus in the specimens.
(Erickson et al., 2015)	Birkigt Triassic sandstone(silicate) Uder	B (?)	10 & 100	?	?	5-25										36,1	40,4	Visible or measurable changes in mineral surfaces and pore fluid composition result from rock interaction

